Cellular and Molecular Life Sciences (2022) 79: 487
https://doi.org/10.1007/s00018-022-04508-7

ORIGINAL ARTICLE

WWOX inhibition by Zfra1-31 restores mitochondrial homeostasis and viability of neuronal cells exposed to high glucose

Cristina Carvalho[1,2,3] · Sónia C. Correia[1,2,3] · Raquel Seiça[4] · Paula I. Moreira[1,2,4,5]

Received: 22 March 2022 / Revised: 26 July 2022 / Accepted: 27 July 2022 / Published online: 19 August 2022

Abstract

Diabetes has been associated with an increased risk of cognitive decline and dementia. However, the mechanisms underlying this association remain unclear and no effective therapeutic interventions exist. Accumulating evidence demonstrates that mitochondrial defects are a key feature of diabetes contributing to neurodegenerative events. It has also been demonstrated that the putative tumor suppressor WW domain-containing oxidoreductase 1 (WWOX) can interact with mitochondria in several pathological conditions. However, its role in diabetes-associated neurodegeneration remains unknown. So, this study aimed to evaluate the role of WWOX activation in high glucose-induced neuronal damage and death. Our experiments were mainly performed in differentiated SH-SY5Y neuroblastoma cells exposed to high glucose and treated (or not) with Zfra1-31, the specific inhibitor of WWOX. Several parameters were analyzed namely cell viability, WWOX activation (tyrosine 33 residue phosphorylation), mitochondrial function, reactive oxygen species (ROS) production, biogenesis, and dynamics, autophagy and oxidative stress/damage. The levels of the neurotoxic proteins amyloid β (Aβ) and phosphorylated Tau (pTau) and of synaptic integrity markers were also evaluated. We observed that high glucose increased the levels of activated WWOX. Interestingly, brain cortical and hippocampal homogenates from young (6-month old) diabetic GK rats showed increased levels of activated WWOX compared to older GK rats (12-month old) suggesting that WWOX plays an early role in the diabetic brain. In neuronal cells, high glucose impaired mitochondrial respiration, dynamics and biogenesis, increased mitochondrial ROS production and decreased mitochondrial membrane potential and ATP production. More, high glucose augmented oxidative stress/damage and the levels of Aβ and pTau proteins and affected autophagy, contributing to the loss of synaptic integrity and cell death. Of note, the activation of WWOX preceded mitochondrial dysfunction and cell death. Importantly, the inhibition of WWOX with Zfra1-31 reversed, totally or partially, the alterations promoted by high glucose. Altogether our observations demonstrate that under high glucose conditions WWOX activation contributes to mitochondrial anomalies and neuronal damage and death, which suggests that WWOX is a potential therapeutic target for early interventions. Our findings also support the efficacy of Zfra1-31 in treating hyperglycemia/diabetes-associated neurodegeneration.

Keywords Diabetes · WWOX · Mitochondria · Zfra1-31 · Neurodegeneration · Neuroprotection

✉ Cristina Carvalho
cristina.im.carvalho@gmail.com;
cristina.carvalho@cnc.uc.pt

✉ Paula I. Moreira
pimoreira@fmed.uc.pt; venta@ci.uc.pt

[1] Center for Neuroscience and Cell Biology, University of Coimbra, 3004-504 Coimbra, Portugal

[2] Center for Innovation in Biomedicine and Biotechnology (CIBB), Coimbra, Portugal

[3] Institute for Interdisciplinary Research, University of Coimbra, Coimbra, Portugal

[4] Institute of Physiology, Faculty of Medicine, University of Coimbra, Coimbra, Portugal

[5] Laboratory of Physiology, Faculty of Medicine, University of Coimbra, 3000-354 Coimbra, Portugal

Introduction

Diabetes is a metabolic disorder with an estimate incidence of over 537 million of people in 2021 according to International Diabetes Federation [1]. Around 90% of all diabetes cases are type 2 diabetes (T2D) and more than 374 millions of people present a high risk to develop this metabolic disease [2]. The uncontrolled raise in diabetes pandemic carries with it enormous health costs due to its complications that include central nervous system damage and an increased risk for cognitive decline and dementia (e.g., vascular dementia and Alzheimer´s disease; AD) [3–7]. To find effective therapeutic targets and strategies, it is crucial to clarify the mechanisms underlying diabetes-associated neurodegeneration.

Previous studies from us and others clearly demonstrate that mitochondria are a mechanistic link between diabetes and brain damage [4, 7–12]. Studies from our laboratory showed that T2D and AD mouse models present similar profiles of cognitive, vascular and mitochondrial abnormalities [4, 13] supporting the hypothesis that T2D enhances the risk of developing AD. More, mitochondrial dysfunction and redox imbalance have been observed in primary cultures of cortical neurons and NT2 neuron-like cells exposed to glucose variations (high/low glucose) and high glucose, respectively [14], as well as in the hippocampus of chemically induced diabetic rats [9]. Nevertheless, mechanistic gaps persist in hyperglycemia/diabetes-associated neurodegeneration hampering the development of effective therapies to prevent this complication.

Besides being a tumor suppressor, WW domain-containing oxidoreductase 1 (WWOX) is a functional participant in molecular interactions, signaling, and apoptosis in many diseases [15]. During apoptosis or stress responses, the cytosolic expression of WWOX increases followed by its translocation to mitochondria and/or nucleus, a process that requires the phosphorylation of WWOX at tyrosine 33 residue [16]. The involvement of WWOX in neurodegenerative conditions has been suggested, however, with contradictory roles [17–20]. For example, a previous study demonstrated that WWOX mediates 1-methyl-4-phenylpyridinium (MPP^+)-induced neuronal death, a model of Parkinson's disease (PD) [18]. In contrast, decreased levels of WWOX were observed in hippocampal neurons of AD human subjects [17]; although an increase in the levels of WWOX phosphorylated at serine 14 residue was associated with AD development [21]. Alterations in WWOX gene (e.g., null and missense mutations) are believed to be involved in the development of severe neural diseases and metabolic disorders [19, 20, 22–25]. However, and as far as we know, there is no published evidence about the involvement of WWOX in hyperglycemia-associated mitochondrial and neuronal damage.

In this line, this study aimed to demonstrate the involvement of activated WWOX in mitochondrial defects observed in neuronal cells exposed to high glucose. In addition, the therapeutic potential of Zinc finger-like protein that regulates apoptosis 31-amino-acid protein (Zfra1-31), the specific inhibitor of WWOX, was also assessed. The experiments were carried out in differentiated SH-SY5Y human neuroblastoma cells exposed to high glucose treated (or not) with Zfra1-31, at two different time points: 3 h (early intervention) and 24 h (late intervention) after glucose exposure. Several parameters were analyzed namely cell viability, WWOX activation (tyrosine 33 residue phosphorylation), mitochondrial membrane potential ($\Delta\Psi m$), mitochondrial respiratory chain parameters, ATP and reactive oxygen species (ROS) production, oxidative stress and damage, mitochondrial biogenesis and dynamics and autophagy-related protein markers. The levels of amyloid β (Aβ) peptide, phosphorylated tau (ptau), synaptic integrity markers and apoptotic cell death were also assessed. The levels of activated WWOX were also determined in brain cortical and hippocampal samples from T2D rats. Overall, our findings show that WWOX activation is a key and early player in high glucose/diabetes-induced neuronal damage and death. Our results also support the therapeutic potential of Zfra1-31 in the treatment of hyperglycemia/diabetes-associated neurodegeneration.

Material and methods

Chemicals

Tetramethylrhodamine methyl ester (TMRM) was obtained from Invitrogen Molecular Probes (Portugal). Protease and phosphatase inhibitors were obtained from Roche Applied Science (Portugal). Substrate for Western blotting, ECF™ and RPN5785 were obtained from GE Healthcare, Portugal. Antibodies manufacturers and dilutions used are described in Table 1. All the other chemicals were of the highest grade of purity commercially available.

Animals' maintenance and characterization

6- and 12-month-old male Wistar and Goto-Kakizaki (GK) rats were housed in our animal colony (Animal Facility, Faculty of Medicine/Center for Neuroscience and Cell Biology, University of Coimbra). The GK rat is a spontaneous, non-obese model of T2D. Rats were maintained under controlled light (12 h day/night cycle) and humidity with free access (except in the fasting period) to water and powdered rodent chow (URF1; Charles River). Animals were anesthetized with ketamine/chlorpromazine [ketamine chloride (75 mg/kg, im, Parke-Davis, Ann Arbor, MI, USA) and

Table 1 Antibodies list

	Dilution	Source	Company/reference
Alexa Fluor 488 anti-rabbit IgG conjugate	1:100	Goat	Life technologies (A11008)
Alexa Fluor 594 anti-mouse IgG conjugated	1:100	Goat	Life technologies (A11005)
β-Actin	1:5000	Mouse	Sigma (A5441)
Autophagy Related 7 (Atg7)	1:1000	Rabbit	Cell Signaling (2631)
B-cell lymphoma 2 (Bcl-2) (50E3)	1:1000	Rabbit	Cell Signaling (2870)
Beclin	1:750	Mouse	BD Transduction (612113)
Dynamin Like Protein-1 (DRP1)	1:1000	Mouse	BD Biosciences (611113)
Phospho-DRP1 (Ser616)	1:1000	Rabbit	Cell Signaling (3455)
Fis1	1:1000	Rabbit	Novus Biologicals (NB100-56646)
LAMP 1 (C54H11)	1:1000	Rabbit	Cell Signaling (3243)
LC3	1:1000	Rabbit	Cell signaling (3868)
MAP2	1:200	Mouse	Millipore (MAB3418)
β-3 Tubulin	1:200	Rabbit	Sigma (T2200)
Mfn1	1:1000	Rabbit	Santa Cruz Biotechnology (sc-50330)
Mfn2	1:1000	Mouse	Santa Cruz Biotechnology (sc-100560)
Mitochondrially encoded cytochrome c oxidase I (COX1/MT-CO1)	1:1000	Rabbit	Cell signaling (62101)
p-mTOR (Ser2448)	1:1000	Rabbit	Cell Signaling (2971)
mTOR	1:1000	Mouse	Cell Signaling (4517)
NADH dehydrogenase subunit 1 (ND1) (C-18)	1:750	Goat	Santa Cruz Biotechnology (sc-20493)
Nuclear factor E2-related factor 1 (NRF1)	1:750	Rabbit	Santa Cruz Biotechnology (sc-33771)
OPA1	1:1000	Mouse	BD Biosciences (612607)
P53(1C12)	1:1000	Mouse	Cell Signaling (2524)
p62	1:1000	Rabbit	Sigma (P0067)
PI3K (class III-D9A5)	1:1000	Rabbit	Cell Signaling (4263S)
PI3K (p110-alpha-C73F8)	1:1000	Rabbit	Cell Signaling (4249S)
Parkin (Prk8)	1:1000	Mouse	Cell Signaling (4211S)
VDAC1/porin	1:750	Rabbit	abcam(ab34726)
Anti-WWOX (phospho Y33)	1:750	Rabbit	Abcam (ab193624
WWOX	1:1000	Rabbit	Merck Millipore (ABN413)
Post synaptic density 95 (PSD95)	1:1000	Rabbit	Cell Signaling (D27E11)
Synaptophysin	1:1000	Mouse	Sigma (S5768)
Synaptosomal-Associated Protein, 25 kDa (SNAP25)	1:750	Mouse	Sigma(S5187)
Succinate Dehydrogenase Subunit A (SDHA)	1:1000	Rabbit	Cell signaling (5839)
p-Tau Antibody (Ser 396)	1:1000	Rabbit	Santa Cruz Biotechnology (sc-101815)
Abeta (6E10)	1:1000	Mouse	Covance (SIG-39300)

chlorpromazine chloride (2.65 mg/kg, im, Lab. Vitória, Portugal)] and sacrificed by decapitation. Immediately before animals' sacrifice, body weight was evaluated, blood glucose levels were determined by a glucose oxidase reaction, using a commercial glucometer (Glucometer–Elite Bayer, Portugal) and compatible reactive tests (Ascencia Elite Bayer, Portugal). Animals' experimentation was performed in accordance with the ARRIVE guidelines, and the European Union and Portuguese legislation (Directive 2010/63/EU; DL113/2013, August 7, respectively), upon approval by the Ethics Committee of the Center for Neuroscience and Cell Biology and Faculty of Medicine, University of Coimbra. Rats' manipulation was performed by qualified persons (accredited by Federation of Laboratory Animal Science Association (FELASA) and Direção Geral de Alimentação e Veterinária, DGAV).

Cells culture, differentiation, and treatment

Human neuroblastoma SH-SY5Y (ECACC; Sigma Aldrich) cells were cultured in 75 cm^2 flasks in Dulbecco's Modified Eagle's medium: nutrient mixture F-12 (DMEM-F12; Gibco-Invitrogen, UK) supplemented with 10% heat-inactivated fetal bovine serum (FBS), 1.2 g/l sodium

bicarbonate; 50 U/ml penicillin and 50 µg/ml streptomycin, in humidified air with 5% CO2 at 37ºC. To perform the experiments, cells were trypsinized (Sigma-Aldrich, USA), counted in a Neubauer chamber using trypan blue and seeded at a density of 50×10^3 cells/well for cell viability and mitochondrial ROS production assays or at 250×10^3 cells/well for Western blot analyses. To obtain cells with morphological and biochemical characteristics of mature neurons, after 24 h of seeding, the cells' medium was renewed to DMEM-F12 supplemented with 1% FBS, 50 U/ml penicillin, 50 µg/ml streptomycin, 50 µg/ml of uridine and 0.11 g/l sodium pyruvate freshly supplemented with 10 µM retinoic acid (RA) for 10 days (Fig. 1) as previously described [26]. In the first set of experiments, differentiated cells were exposed to DMEM-F12 medium supplemented with 10- or 25-mM glucose during 24 h or 48 h. Differentiated cells exposed to DMEM-F12 medium without glucose supplementation were used as control cells. In the second set of experiments, differentiated cells were incubated with 25 mM glucose for 48 h and exposed to 20 µM Zfra1-31 peptide (Genemed synthesis, mssrrsssckyceqdfrahtqknaatpfla $n > 95\%$) 3 h (early intervention; EI) or 24 h (late intervention; LI) after glucose incubation (Fig. 1) after the beginning of glucose incubation. Cells not exposed to Zfra1-31 were also used as control cells.

MTT assay for cell viability

After the appropriate incubations, cells seeded in 24-multiwell plates were incubated with 3-(4,5-dimethylthiazol-2-yl)-2,5-diphenyltetrazolium bromide (MTT) substrate for 2 h [27]. Viable cells with active metabolism converted MTT into an insoluble purple colored formazan product, which was solubilized by acidified isopropanol. The quantity of formazan was measured by recording changes in absorbance at 570 nm using a spectrophotometer SpectraMax Plus 384, being the quantity of formazan directly proportional to the number of viable cells. The results were expressed as percentage of control absorbance for each individual experiment.

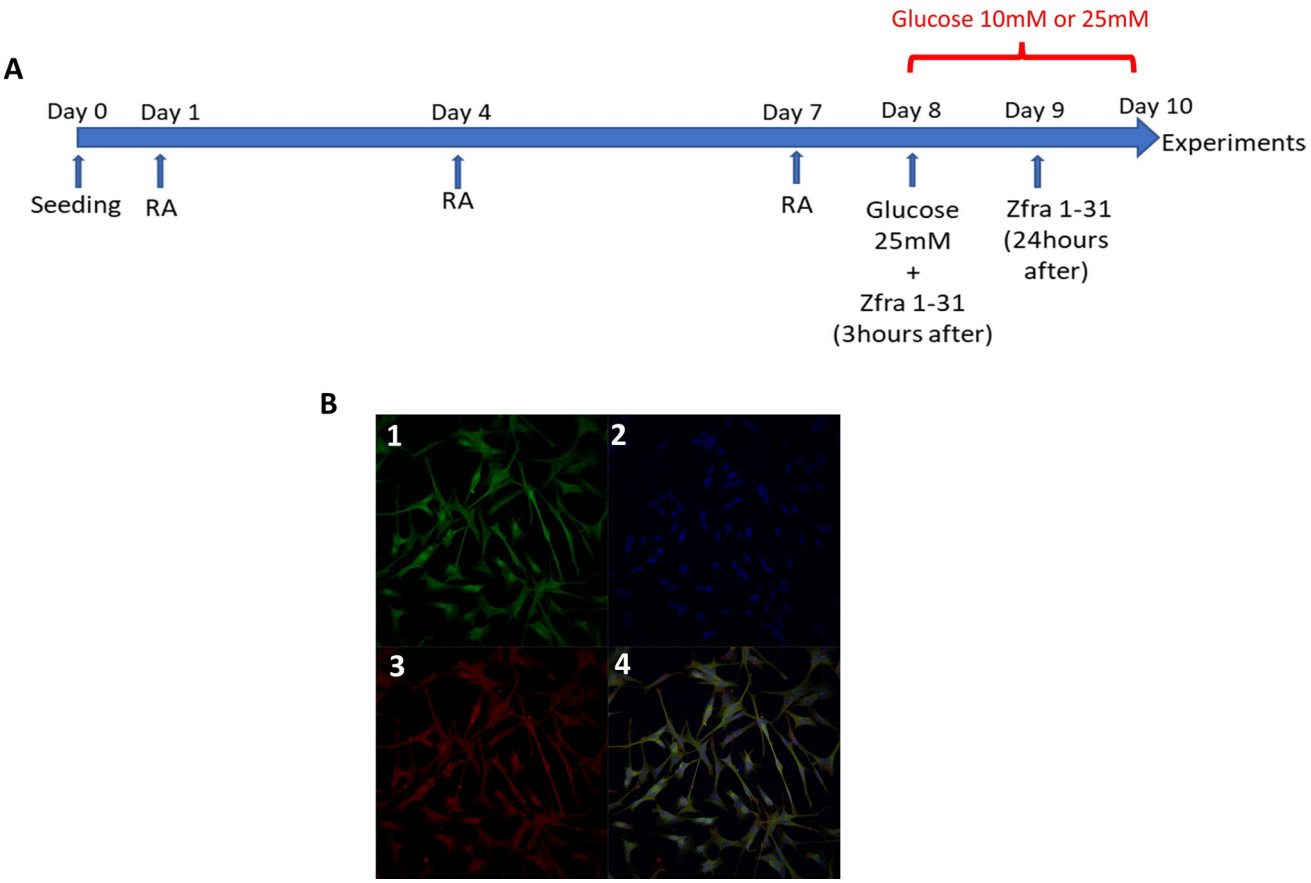

Fig. 1 Experimental design and characterization of differentiated SH-SY5Y cells. **A** Timeline of experimental protocol; **B.1** β-III tubulin (microtubule element of the tubulin family found almost exclusively in neurons); **B.2** Hoechst (used for specifically staining the nuclei of living or fixed cells or tissues); **B.3** MAP2 (neuron-specific cytoskeletal proteins enriched in dendrites and perikaryal); **B.4**. Representative images of 3 independent experiments. *MAP2* microtubule-associated protein 2, *RA* retinoic acid

Measurement of mitochondrial membrane potential

Mitochondrial membrane potential ($\Delta\Psi m$) was determined using the cationic fluorescent probe tetramethylrhodamine methyl ester ($TMRM^+$, #T668; Molecular probes), which accumulates predominantly in polarized mitochondria [28]. After treatments, differentiated SH-SY5Y cells were washed with phosphate buffer saline (PBS) and incubated with DMEM phenol free medium (Gibco-Invitrogen, UK) supplemented with 3.15 g/l glucose, 1% heat-inactivated FBS, 1.2 g/l sodium bicarbonate, 1% penicillin/streptomycin, 0.11 g/l sodium pyruvate and 50 µg/ml uridine containing 300 nM $TMRM^+$ for 1 h at 37 °C. Basal fluorescence (540 nm excitation and 590 nm emission wavelengths, with a cutoff at 590 nm) was measured using a SpectraMax GEMINI EM fluorometer (Molecular Devices) every 30 s for a total of 3 min. After, carbonilcyanide p-triflouromethoxyphenylhydrazone (FCCP; 1 µM) and oligomycin (2 µg/ml) were added to the medium, which contributed to maximal mitochondrial depolarization. Fluorescence (540 nm excitation and 590 nm emission wavelengths, with a cutoff at 590 nm) was measured once more, every 30 s for a total of 3 min. The difference between the increase of $TMRM^+$ fluorescence upon addition of FCCP plus oligomycin and basal fluorescence values was used to evaluate $\Delta\Psi$m. The results were expressed as percentage of control fluorescence for each individual experiment.

Measurement of mitochondrial reactive oxygen species

The presence of hydrogen peroxide (H_2O_2) within the mitochondria was determined using the selective mitochondrial fluorescent probe MitoPY1 (Tocris Bioscience™, #44-281-0), which allows to detect the presence of H_2O_2 within the mitochondria [29]. Briefly, 1 h before the end of the incubation period, cells were incubated with 10 µM MitoPY1 at 37 °C. After the incubation, cells were washed with warm PBS and placed in DMEM phenol free medium (Gibco-Invitrogen, UK) supplemented with 3.15 g/l glucose, 1% heat-inactivated FBS, 1.2 g/l sodium bicarbonate, 1% penicillin/streptomycin, 0.11 g/l sodium pyruvate and 50 µg/ml uridine, and the fluorescence was read for 30 min (excitation 503 nm, emission 540 nm) using a microplate reader spectrofluorometer Gemini EM (Molecular Devices, USA). MitoPY1 fluorescence was expressed as percentage of control for each individual experience. The mitochondrial complex III inhibitor, antimycin A (AA), was used as positive control for mitochondrial ROS production.

Evaluation of carbonyl groups levels

Carbonyl groups were determined according to Colombo et al. [30], with slight modifications. Briefly, 50 µg of each sample were incubated with 10 mM 2,4 dinitrophenylhydrazine (DNPH) solution, vortex-mixed and incubated in the dark at room temperature (RT) for 60 min, with vortex-mixing every 10–15 min. At the end of the incubation period, 20% of trichloroacetic acid (TCA) solution was added to the protein samples and incubated on ice for 15 min. Then, samples were centrifuged at 10,000×*g* in a tabletop microcentrifuge for 5 min, at 4 °C. Then, supernatants were discarded and protein pellets were washed with 1 ml of 20% TCA vortex-mix, and centrifuged at 10,000×*g* for 5 min, at 4 °C. Supernatants were discarded and protein pellets were washed with 1 ml of 1:1 (v/v) ethanol:ethyl acetate and mix by to remove any free DNPH. Those wash steps were repeated at least twice until the supernatants were completely transparent and then, the pellets were collected by centrifugation at 10,000×*g* for 5 min, at 4 °C. The final pellets were left to dry for about 5 min to allow complete solvent evaporation and then they were resuspended in 1 ml of 6 M guanidine hydrochloride (dissolved in 50 mM phosphate buffer, pH 2.3) and incubated at 37 °C for 15–30 min with vortex mixing. The carbonyl content was evaluated from the maximum absorbance, at 360 nm, measured in a SpectraMax Plus 384 multiplate reader, and calculated using a molar absorption coefficient (ε) at 360 nm = 22×103 M^{-1} cm^{-1}. The results were expressed as µmol/mg protein.

Nitrite levels

Nitrite levels were determined indirectly in the samples through the nitric oxide (NO•) production upon reaction with the Griess reagent, according to Green et al. [31]. Briefly, 125 µl of the cells' medium were incubated, for 10 min, in 125 µl Griess reagent (containing 1% sulfanilamide in 2.5% phosphoric acid, plus 0.1% *n*-(1-naphthyl) ethylenediamine dihydrochloride), protected from light. Then, the absorbance of the medium was read at 550 nm, in a SpectraMax Plus 384 multiplate reader. The nitrite content was calculated using a standard curve of sodium nitrite. Results were expressed as µM.

Measurement of thiobarbituric acid reactive substances (TBARS) levels

TBARS levels were determined using the thiobarbituric acid (TBA) assay, according to a modified procedure described by Ernster and Nordenbrand [32]. Briefly, 50 µg of each sample were incubated in 250 µl of reaction medium (175 mM KCl; 10 mM Tris–HCl; pH 7.4), at 37 °C. The reaction was started

with the addition of 1 mM ADP/0.1 mM Fe^{2+} and stopped after 15 min with the addition of 250 µl of 40% TCA. Then, 1 ml of 0.67% TBA was added to each sample, vortex-mixed and boiled for 15 min, at 100 °C. Samples were centrifuged at 18,000×*g* for 10 min and the absorbance of the supernatants were measured at 530 nm. The amount of TBARS was calculated using a molar coefficient of $1.56 \times 105\ M^{-1}\ cm^{-1}$ and expressed as nmol TBARS/mg protein.

Seahorse XF24 extracellular flux analyzer measurements

Mitochondria oxygen consumption rate (OCR) was evaluated by seeding approximately 15,000 cells per well in the 24-well cell culture microplates provided by the manufacturer (Agilent, Santa Clara, CA, USA; Cat. No. 100777-004), as previously described [33]. Briefly, after cells differentiation and treatments, and 1 h before placing the culture microplates in the Seahorse analyzer, the cells were washed in unbuffered DMEM from Sigma Chemical Co (St. Louis, MO, USA; Cat. No. 5030) supplemented with 25 mM glucose, 1.82 mM sodium pyruvate, and 0.2 mM L-glutamine, without HEPES and sodium bicarbonate, at pH 7.4. OCR measurements were made using a 1 min mix, 30 s wait, and 3 min read cycling protocol. During the first 3 reading periods, basal OCRs were determined. After the third reading, 1 µM of oligomycin was injected to the wells and the resulting OCR was measured over 3 reading cycles. After this, two injections of 2 µM FCCP were performed and for each injection the OCR was recorded over 3 cycles. Finally, a mixture of rotenone (2 µM) and AA (2 µM) was injected into the wells and the resultant OCR was measured over 3 reading cycles. Rotenone (a mitochondrial complex I inhibitor) and AA (a mitochondrial complex III inhibitor) were used to inhibit mitochondrial respiration allowing the determination of the non-mitochondrial OCR. To calculate the basal mitochondrial OCR, the non-mitochondrial OCR is subtracted from the OCR obtained before the addition of oligomycin (inhibits the mitochondrial ATP synthase). To evaluate the maximal respiratory capacity, we subtracted the non-mitochondrial OCR from the OCR following FCCP addition (disrupts ATP synthesis by dissipating the proton gradient). To obtain the spare respiratory capacity, we subtracted the basal mitochondrial OCR from the maximal respiratory capacity. The mitochondrial ATP production was assessed after oligomycin addition, by subtracting the non-mitochondrial OCR from the OCR value after oligomycin addition.

Caspase 3 activity

Caspase 3 activity was measured using a colorimetric method, as previously described [34]. Briefly, 25 µg of total protein lysate were incubated, at 37 °C for 2 h, in 25 mM Hepes, pH 7.5 containing 0.1% CHAPS, 10% sucrose, 2 mM DTT, and 40 µM Ac-DEVD-pNA. Caspase 3-like activity was determined by measuring substrate cleavage at 405 nm in a microplate spectrophotometer SpectraMax Plus 384 (Molecular Devices, USA). Values were expressed as percentage of control for each individual experiment.

Cells' protein extraction for Western blot analysis

After the proper incubations, cells were lysed by adding 50 µl lysis buffer (Cell Signaling #9803) supplemented with protease inhibitors (cOmplete™, Mini, EDTA-free Protease Inhibitor Cocktail from Roche, #04693159001), phosphatase inhibitors (commercial phosphatase inhibitor cocktail, PhosSTOP™, from Roche, #4906837001), 0.1 M phenylmethanesulfonyl fluoride (PMSF) (Sigma, #10837091001) and 0.2 M dithiothreitol (DTT) (Sigma, #D9163). The mixture was frozen 3 times in liquid nitrogen to favor cells disruption, centrifuged at 18,000×*g* (Eppendorf centrifuge 5415C) for 10 min, at 4 °C, as previously described [35]. The supernatants represent the cytosolic fractions and the resulting pellets the membrane fractions. The protein concentration of the samples was determined with the Pierce ™ BCA Protein Assay Kit (Thermo Fisher, #23227).

Brain tissue processing for Western blot analysis

After the sacrifice of the animals, the brains were quickly removed, and the cerebral cortexes were dissected on ice, flash-frozen using liquid nitrogen and stored at − 80 °C [35]. For the Western blot analysis, a small portion of the brain cortex and hippocampus was homogenized in 1 × lysis buffer (Cell Signaling # 9803), supplemented with 0.1 M PMSF, 0.2 M DTT, and protease and phosphatase inhibitors (Roche Applied Science). Samples were then incubated on ice for 15 min, frozen and defrozen 3 times to favor disruption, centrifuged at 18,000*g* (Eppendorf centrifuge 5415C) for 10 min, at 4 °C, and the resulting supernatants were collected, and protein concentration was determined with the Pierce ™ BCA Protein Assay Kit (Thermo Fisher, #23227).

Western blot analysis

As previously described [35], samples (30–50 µg/lane), obtained from total lysate extracts or brain cortical and hippocampal homogenates, were resolved by electrophoresis in 8–15% SDS—polyacrylamide gels and transferred to previously activated polyvinylidene difluoride (PVDF) membranes (Merck Millipore Ltd., #IPVH00010), for 2 h at 0.75 mA. Afterwards, non-specific binding was blocked by gently agitating the membranes for 1 h in 5% BSA and 0.1% Tween in TBS (TBS-T), at RT, and incubated overnight at 4 °C with

the specific primary antibodies (Table 1). After washing three times (5 min each) with TBS-T, each membrane was incubated with secondary antibodies for 1 h, at RT. Finally, and after washing three times (5 min each) with TBS-T, membranes were incubated for a maximum period of 5 min with the enhanced chemifluorescent (ECF) detection system (GE Healthcare, #GEHERPN5785), and the immunoreactive bands were visualized using a Chemidoc Imaging System (Bio-Rad). β-actin was used as a loading control, and bands density was evaluated with the Quantity One Software (Bio-Rad).

Membranes re-probing

In some cases, membranes were re-probed instead of running and blotting multiple gels, to maximize sample yield (e.g., loading control probes). Briefly, membranes were washed for 30 min with 40% methanol for ECF removal followed by a 30 min washing in TBS-T. The stripping protocol was performed with a 5 min wash with pure water followed by 10 min stripping with 200 mM NaOH. Next, membranes were washed for 5 min with pure water and then the non-specific binding was blocked by gently agitating the membranes for 1 h in 5% BSA in TBS-T, at RT, and incubated overnight, at 4 °C, with the specific primary antibodies. Then, the last steps of Western blot protocol were performed as described above.

Statistical analysis

The statistical analysis was performed using the GraphPad Prism 8.0.2 software (San Diego, CA, USA) and presented as mean ± standard error of the mean (SEM). All the experiments were performed in 4–8 independent assays. Normality tests were performed using the Shapiro–Wilk test. The statistical significance was determined using the one-way ANOVA when normal distribution was observed or using the Kruskal–Wallis test, in the remaining cases. Statistical significance was considered at $p < 0.05$.

Results

Characterization of diabetic rats

GK rats presented a significant decrease in body weight (~ 20%) and a significant increase in occasional blood glucose (~ 85%) levels (Table S.1) compared to the respective control counterparts.

Increased levels of activated WWOX in brain cortex and hippocampus of diabetic rats and neuronal cells exposed to high glucose

We evaluated the levels of WWOX phosphorylated at tyrosine 33 residue (tyr33; activated WWOX) in brain cortex and hippocampus from 6- and 12-month-old GK and age-matched control rats. A significant increase in brain cortical (~ 20%) and hippocampal (twofold) pWWOX (tyr33) levels was observed in 6-month-old GK rats, when compared with age-matched control rats (Fig. 2A, B). However, in 12-month-old GK rats, a decrease (~ 20%) in pWWOX (tyr33) levels is observed in brain cortex (Fig. 2A) while no significant differences were detected in the hippocampus (Fig. 2B), when compared to the younger GK rats. These observations suggest that WWOX is activated at early ages and before overt mitochondrial defects, as previously reported [10, 36].

In neuronal cells exposed to 25 mM glucose we observed a significant increase (~ 79%) in pWWOX (tyr33) levels at 24 h of incubation (Fig. 2C), being this increase maintained at 48 h of incubation. A ~ 60% increase in pWWOX (tyr33) levels was also observed in cells exposed to 10 mM glucose however, this increase was only statistically significant after 48 h of incubation. Interestingly, the alterations in pWWOX levels occurred before the decrease (~ 15%) in cell viability, which occurred only at 48 h of incubation in the presence of both glucose concentrations (Fig. 2D). Additionally, WWOX activation preceded mitochondrial dysfunction and the increased production of ROS (SFig. 1). Together, these results suggest that WWOX activation is an early event in neuronal dysfunction associated to hyperglycemia/diabetes.

The inhibition of WWOX activation by Zfra1-31 protects against high glucose-induced cell death

Based on the observations described above, we decided to perform the subsequent experiments in neuronal cells incubated with 25 mM glucose for 48 h. To test the efficacy of the pharmacological inhibition of WWOX by Zfra1-31, we selected two time-points to mimic an early intervention (EI—Zfra1-31 was incubated 3 h after high glucose exposure) and a late intervention (LI—Zfra1-31 was incubated 24 h after high glucose exposure; Fig. 1). We observed that Zfra1-31 diminished (~ 64%) the levels of activated WWOX (pWWOX tyr33) (Fig. 3A) and

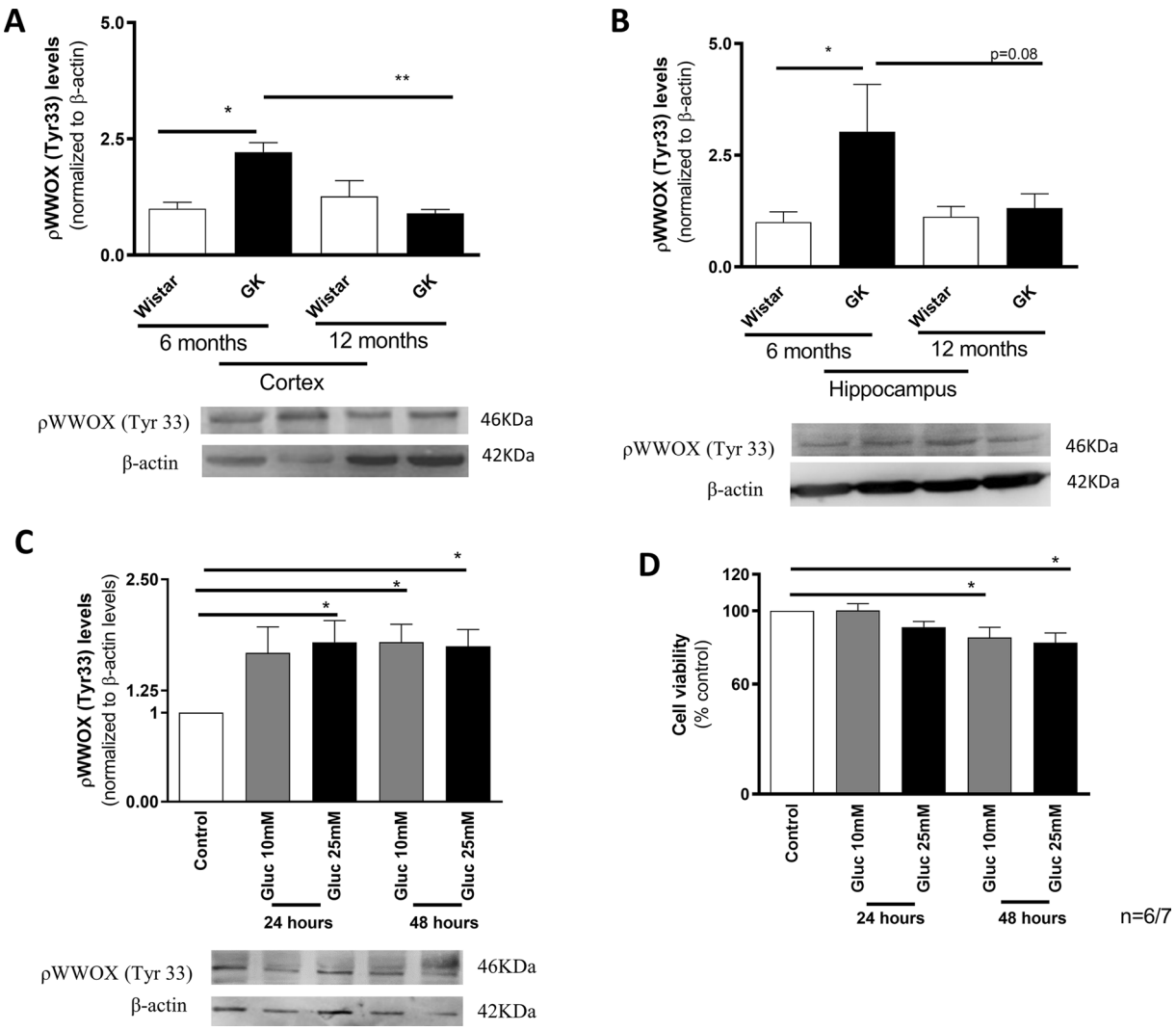

Fig. 2 WWOX activation levels in brain cortex of Goto-Kakisaki (GK) rats and neuronal cells exposed to high glucose. ρWWOX (tyr 33) levels in brain cortical (**A**) and hippocampal (**B**) samples from 6- and 12 month-old Wistar control and GK rats and in cells extracts (**C**), with representative blots, and cell viability of neuronal cells exposed to high glucose (**D**). Data represent mean ± SEM from 6 independent animals or 6 independent cells experiments (in triplicates, except for Western blot experiments), respectively. Statistical significance: $*p < 0.05$ when compared with control counterparts. *GK* Goto Kakizaki, *WWOX* putative tumor suppressor WW domain-containing oxidoreductase 1

significantly increased cell viability (~ 16%; Fig. 3B). It was previously described that pWWOX (tyr33) can form a complex with p53 that migrates to mitochondria causing caspases activation [16]. Accordingly, we observed that high glucose significantly increased p53 levels (~ 58%) as well as caspase 3 activity (~ 44%), being these alterations reduced by Zfra1-31 (~ 34 (LI)—47(EI) % and 21 (LI)—50 (EI) %, respectively) (Fig. 3C, D). Concerning Zfra1-31 time-points, as noted above, the EI condition seems to be more effective than the LI condition.

The inhibition of WWOX activation by Zfra1-31 protects against high glucose-induced mitochondrial dysfunction

Mitochondria are crucial for the generation of energy (ATP) required for the normal functioning of neuronal

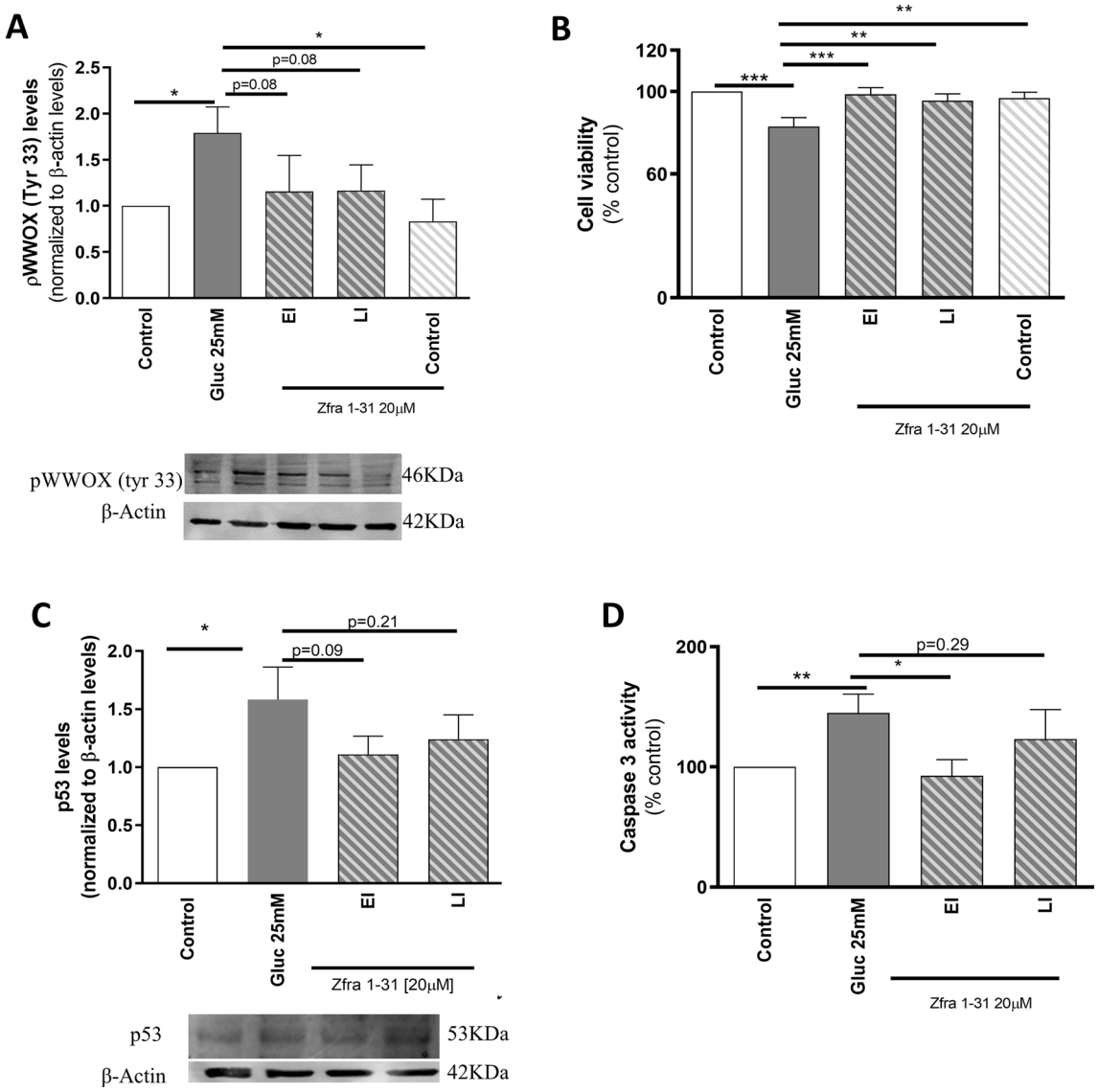

Fig. 3 ρWWOX (tyr33) inhibition by Zfra1-31 prevents high glucose-induced cell death, and increased p53 levels and caspase 3 activity. **A** ρWWOX (tyr 33) levels; **B** cell viability; **C** p53 levels and western blot representative image; **D** Caspase 3 activity. Data shown represent mean ± SEM from 4/6 independent experiments (in triplicates, except for Western blot experiments). Statistical significance: $*p < 0.05$ and; $**p < 0.01$ when compared with respective control condition. *WWOX* putative tumor suppressor WW domain-containing oxidoreductase 1, *EI* early intervention; LI- late intervention

cells. As demonstrated in Fig. 4A, B, high glucose caused a significant decrease (~ 34%) in mitochondrial membrane potential ($\Delta\Psi m$) and a significant increase (~ 50%) in mitochondrial ROS production. The Seahorse analyses revealed that cells exposed to high glucose presented a decrease (~ 35%) in basal mitochondrial respiration (Fig. 4C), as demonstrated by OCR in the absence of mitochondrial inhibitors, a decrease (~ 31%) in maximal O_2 consumption (Fig. 4D), which indicates the maximal O_2 consumption rate attained by adding the uncoupler FCCP, and a decrease (~ 50%) in spare respiratory capacity (Fig. 4G), described as the amount of extra ATP that can be produced by OXPHOS in case of a sudden increase in energy demand. More, we observed a significant increase (~ 40%) in proton leak (Fig. 4E), which was determined in the presence of the ATP synthase inhibitor oligomycin; in this situation the mitochondrial oxygen consumption is due to ATP synthase-independent leakage of protons from the intermembrane space to the mitochondrial matrix causing a decrease (~ 24%) in mitochondrial coupling efficiency (Fig. 4H) and, consequently, a decrease (~ 42%) in ATP production (Fig. 4F). Interestingly, Zfra1-31, in both EI and LI conditions, normalized mitochondrial proton leak by decreasing it ~ 65–70%, respectively (Fig. 4E). In

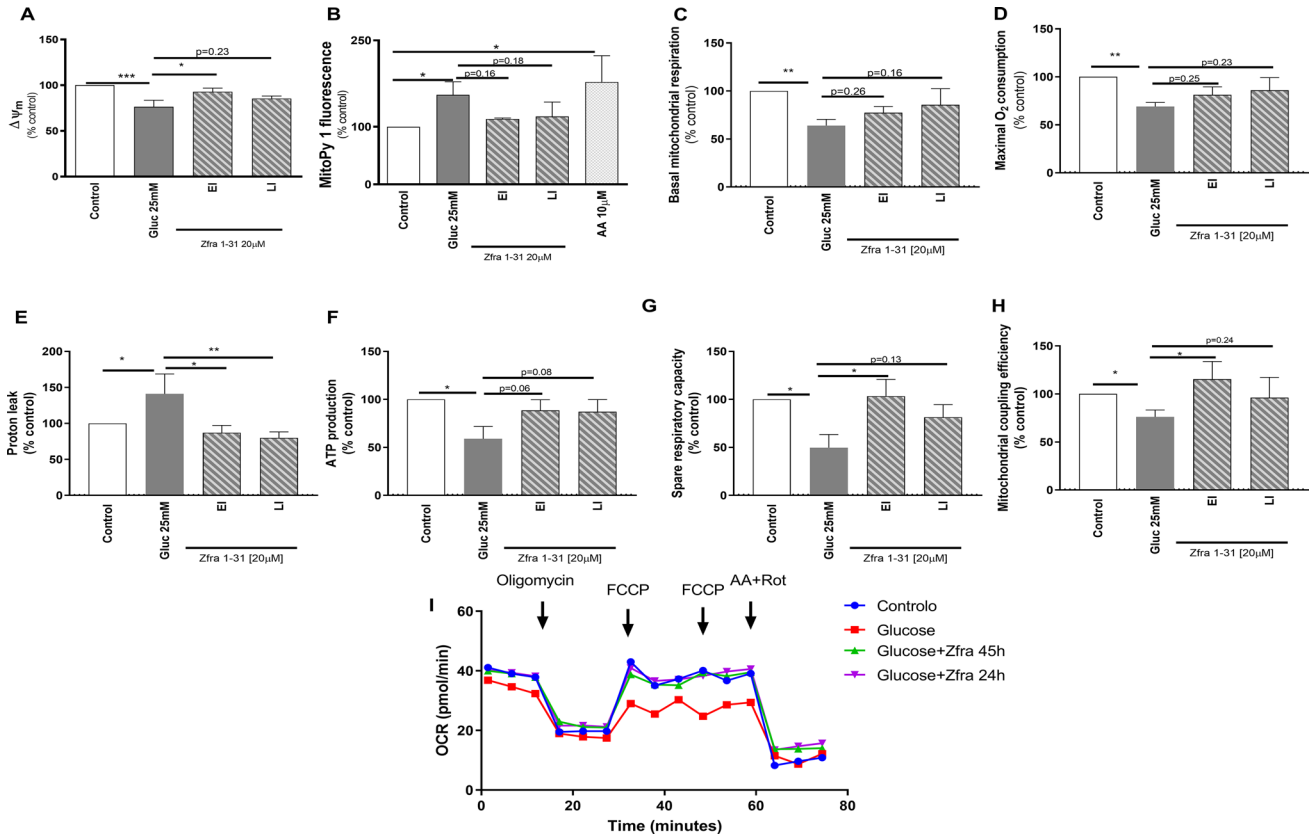

Fig. 4 ρWWOX (tyr33) inhibition by Zfra1-31 rescues mitochondrial respiratory chain function. **A** $\Delta\Psi m$; **B** mitochondrial ROS production; **C** basal mitochondrial respiration; **D** maximal O_2 consumption; **E** proton leak; **F** ATP production; **G** spare respiratory capacity; **H** mitochondrial coupling efficiency; **I** representative Seahorse analysis graph. Data shown represent mean ± SEM from 4/6 independent experiments. Statistical significance: $*p < 0.05$; $**p < 0.01$ when compared with respective condition. *WWOX* putative tumor suppressor WW domain-containing oxidoreductase 1, *EI* early intervention, *LI* late intervention, $\Delta\Psi m$ mitochondrial membrane potential, O_2 oxygen, *FCCP* carbonyl cyanide-p-trifluoromethoxyphenylhydrazone, *AA* antimycin A, *Rot* rotenone, *OCR* oxygen consumption rate

the EI condition, Zfra1-31 also increased $\Delta\Psi m$ (~ 15%) (Fig. 4A), spare respiratory capacity (~ 30%) (Fig. 4G) and mitochondrial coupling efficiency (~ 39%) (Fig. 4H). The remaining parameters were also improved by Zfra1-31, in both EI and LI conditions, but those effects did not achieve statistical significance (Fig. 4).

The inhibition of WWOX activation by Zfra1-31 protects against high glucose-induced oxidative stress and damage

Neuronal cells are highly sensitive cells and even slight changes in mitochondrial function may have a profound impact on cellular homeostasis. Under our experimental conditions, we observed a ~ 90% increase in the levels of carbonyl groups in cells exposed to high glucose (Fig. 5A). Protein carbonyl groups, a marker of protein oxidation, are considered sensitive and reliable biomarkers of oxidative stress and damage due to their early formation and to the relative stability of carbonylated proteins [37]. TBARS are a by-product of lipid peroxidation, and their measurement is generally used to evaluate lipid oxidation in cells and tissue extracts. Under our experimental conditions, high glucose promoted a ~ 10% increase in TBARS levels when compared with the control condition (Fig. 5B). Furthermore, a slight increase in nitrite levels (Fig. 5B), a marker of nitrosative stress, was observed under high glucose conditions. Interestingly, Zfra1-31, in both EI and LI conditions, reduced high glucose-induced alterations, being this reduction more pronounced in the EI condition (Fig. 5). Indeed, in EI condition we observed a twofold reduction in carbonyl group levels when compared with high glucose condition. LI condition was also able to reduce the levels of carbonyl groups, although it did not reach statistical significance. Regarding TBARS levels, the EI condition promoted a twofold reduction in the levels of this lipid peroxidation marker. A slight

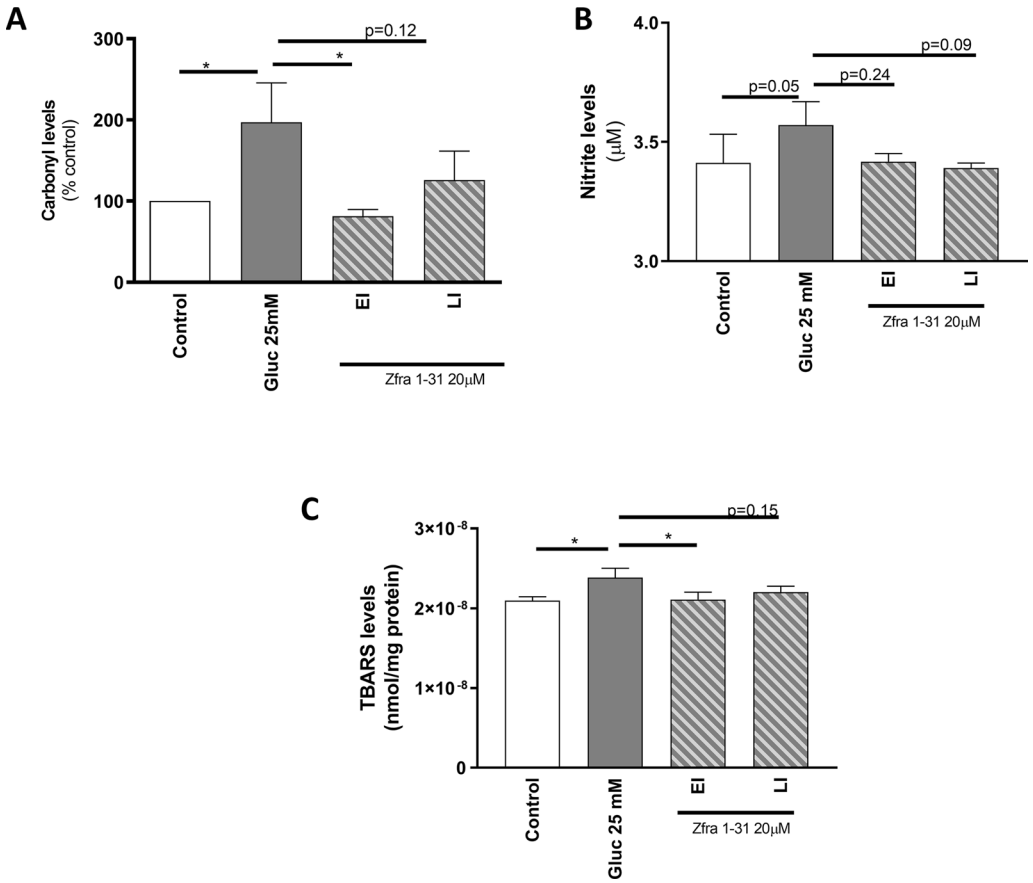

Fig. 5 ρWWOX (tyr33) inhibition by Zfra1-31 ameliorates oxidative stress/damage **A** carbonyl groups **B** nitrite and **C** TBARS levels. Data shown represent mean ± SEM from 4/6 independent experiments. Statistical significance: $*p < 0.05$ when compared with respective condition. TBARS- Thiobarbituric acid reactive substances

reduction of TBARS levels was also observed in LI condition. Also, Zfra1-31 in both EI and LI conditions, caused a non-statistical reduction in nitrite levels.

The inhibition of WWOX activation by Zfra1-31 restores mitochondrial dynamics under high glucose conditions

The maintenance of a healthy pool of mitochondria results from a complex interplay and strict balance between several mechanisms. This balance is necessary to protect mitochondria against stress, to regulate mitochondrial shape, function, and mass, to monitor mitochondrial damage and to ensure the selective removal of dysfunctional mitochondrial proteins or entire organelles [38]. In this context, we evaluated the levels of key proteins involved in mitochondrial biogenesis, and fusion/fission and autophagic clearance under high glucose conditions and in the presence of Zfra1-31. Concerning fission/fusion events, which are essential to modulate mitochondrial shape, we observed that high glucose caused an imbalance in these events. In relation to mitochondrial fusion, a significant decrease (~34%) in mitofusin (Mfn) 1 (Fig. 6A) and a significant increase (~41%) in optic atrophy 1 (Opa-1) levels (Fig. 6C) were observed. Concerning mitochondrial fission, a significant decrease (~34%) in phospho-dynamin-related protein 1 (pDRP1)/DRP1 (Fig. 6D) was observed. Also, a non-statistically significant increase in mitochondrial fission 1 protein (Fis1) and Mfn2 (Fig. 6B, E) levels were observed in cells exposed to high glucose. These results suggest that hyperglycemia/diabetes causes an imbalance in mitochondrial dynamics. Importantly, the inhibition of pWWOX (tyr33) by Zfra1-31 in EI condition normalized the levels of pDRP1/DRP1, by increasing it ~ 35% (Fig. 6D), and of OPA1, by decreasing it ~ 27% (Fig. 6C), when compared with high glucose condition. Importantly, Zfra-131 in LI condition also caused a ~ 15% increase in pDRP1/DRP1 and ~ 25% decrease in OPA1 levels, when compared with high glucose condition.

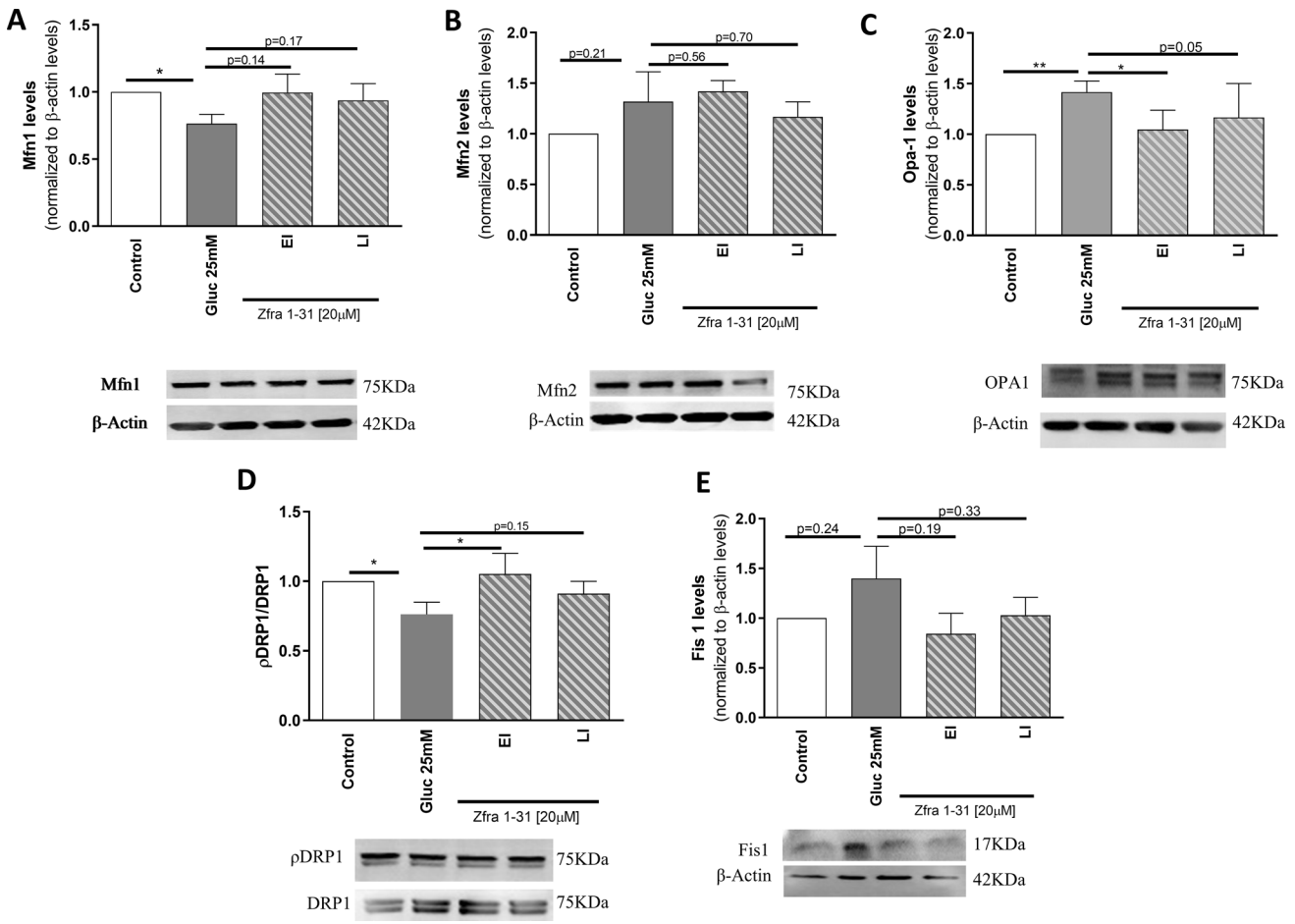

Fig. 6 ρWWOX (tyr33) inhibition by Zfra1-31 ameliorates mitochondrial dynamics **A** Mfn1 levels and representative western blot image; **B** Mfn2 levels and representative Western blot image; **C** Opa-1 levels and representative Western blot image; **D** ρDRP1/DRP1 levels and representative Western blot image and; **E** Fis1 levels and representative Western blot image. Data shown represent mean ± SEM from 4/6 independent experiments. Statistical significance: $*p < 0.05$; $**p < 0.01$ when compared with respective condition. *WWOX* putative tumor suppressor WW domain-containing oxidoreductase 1, *EI* early intervention, *LI* late intervention, *Mfn* mitofusin, *DRP1* dynamin-related protein 1, *Fis1* mitochondrial fission 1 protein, *Opa-1* optic atrophy type 1

In relation to the other parameters, Zfra1-31 in both EI and LI conditions, partially normalized the levels of the proteins (Fig. 6).

The inhibition of WWOX activation by Zfra1-31 restores mitochondrial biogenesis under high glucose conditions

It was previously shown that under diabetic conditions an increase in mitochondrial biogenesis seems to occur [39]. Indeed, increased mitochondrial biogenesis represents a cellular response against elevated oxidative stress aiming to attenuate damage through the regulation of mitochondrial metabolism and ROS production [40]. Accordingly, in the presence of high glucose we observed a significant increase in the levels of biogenesis-related proteins namely in the nuclear respiratory factor 1 (NRF1; ~ 28%) (Fig. 7E), in the mitochondrially encoded subunits cytochrome C oxidase I (MTCO1; ~ 53%) (Fig. 7A) and in the succinate dehydrogenase complex flavoprotein subunit A (SDHA; ~ 69%) (Fig. 7D). Functional mitochondria rely on the proper assembly of different subunits and our results show that this may not occur under high glucose conditions. Indeed, it was observed a decrease in the levels of mitochondrial encoded NADH-ubiquinone oxidoreductase chain 1 (ND1; ~ 41%) and of voltage-dependent anion channel (VDAC; ~ 47%) (Fig. 7B, C), essential proteins in the formation of the mitochondrial respiratory chain complexes. Together, these observations suggest a mitochondrial network imbalance in cells exposed to

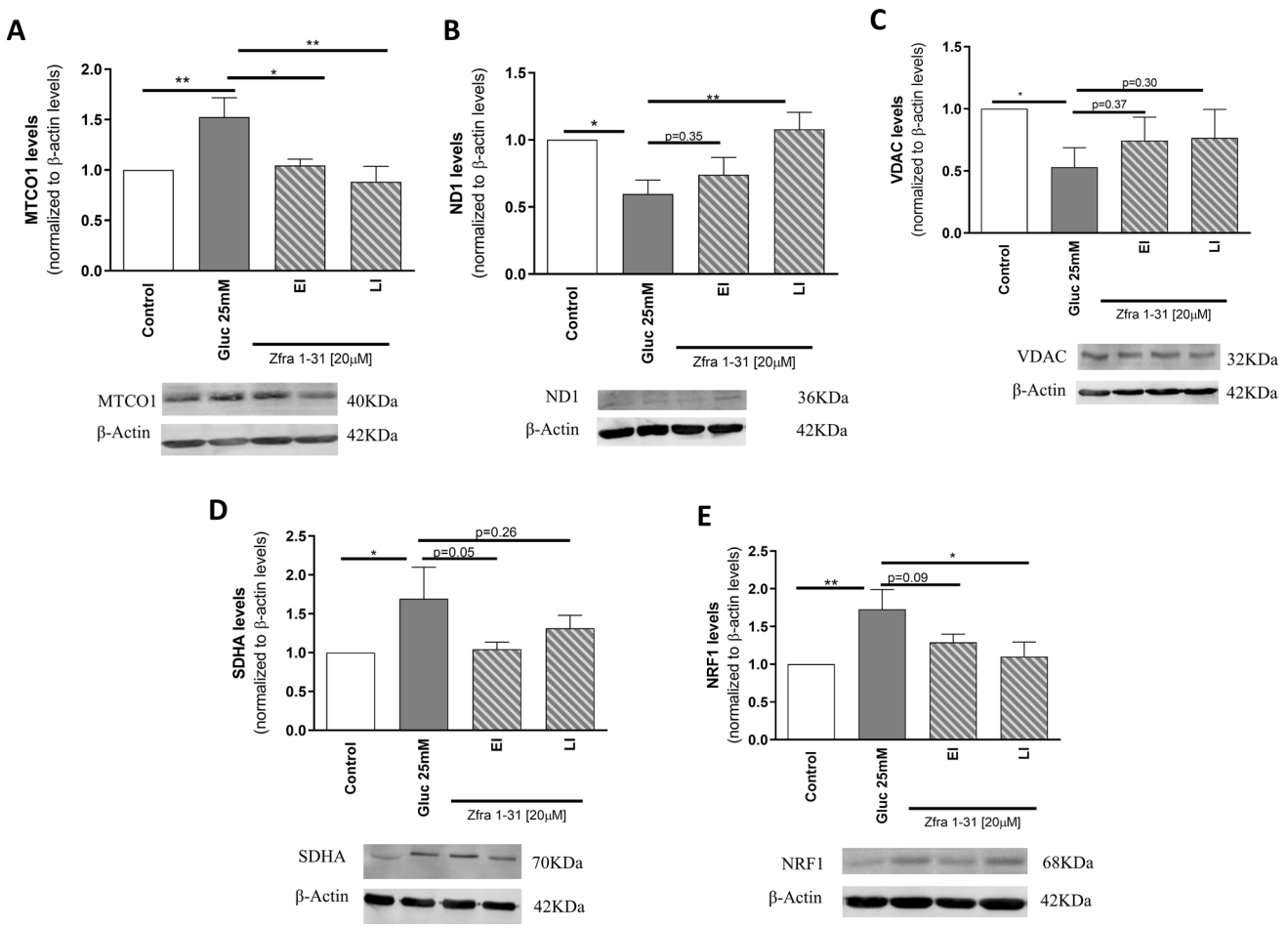

Fig. 7 ρWWOX (tyr33) inhibition by Zfra1-31 partially rescues mitochondrial biogenesis. **A** MTCO1 levels and representative Western blot image; **B** ND1 levels and representative Western blot image; **C** VDAC levels and representative Western blot image; **D** SDHA levels and representative Western blot image; **E** NRF1 levels and representative Western blot image. Data shown represent mean ± SEM from 4/6 independent experiments. Statistical significance: $*p < 0.05$; $**p < 0.01$ when compared with respective condition. *WWOX* putative tumor suppressor WW domain-containing oxidoreductase 1, *EI* early intervention, *LI* late intervention, *MTCO1* mitochondrially encoded cytochrome C oxidase I, *ND1* NADH-ubiquinone oxidoreductase chain 1, *VDAC* voltage-dependent anion channel, *SDHA* succinate dehydrogenase complex flavoprotein subunit A, *NRF1* nuclear respiratory factor 1

high glucose. Again, Zfra1-31 normalized the alterations caused by high glucose. Particularly, in both EI and LI conditions, Zfra1-31 significantly reduced (~ 52 and 64%, respectively) the levels of MTCO1 (Fig. 7A) and, in LI condition, Zfra1-31 significantly increased (42%) ND1 and reduced (~ 62%) NRF1 levels. In relation to the other proteins, a partial recovery (ranging from 20 to 40%) was observed in the presence of Zfra1-31 (Fig. 7) suggesting that this compound contributes to mitochondrial homeostasis.

The inhibition of WWOX activation by Zfra1-31 tends to normalize mito/autophagy under high glucose conditions

The accumulation of dysfunctional mitochondria can result from a defective clearance by autophagy. We observed that autophagy is compromised in several steps. Although we did not observe significant alterations in the levels of phosphorylated mammalian target of rapamycin (pmTOR)/mTOR (Fig. 8A), a significant decrease (~ 35%) in the levels of phosphatidylinositol-4,5-bisphosphate 3-kinase (PI3K) (p110), a kinase responsible for the phosphorylation of mTOR, was observed under high glucose conditions (Fig. 8B). Regarding the nucleation phase of autophagy, which relies in the formation of a beclin/parkin/PI3K class III complex, some disturbances were also observed.

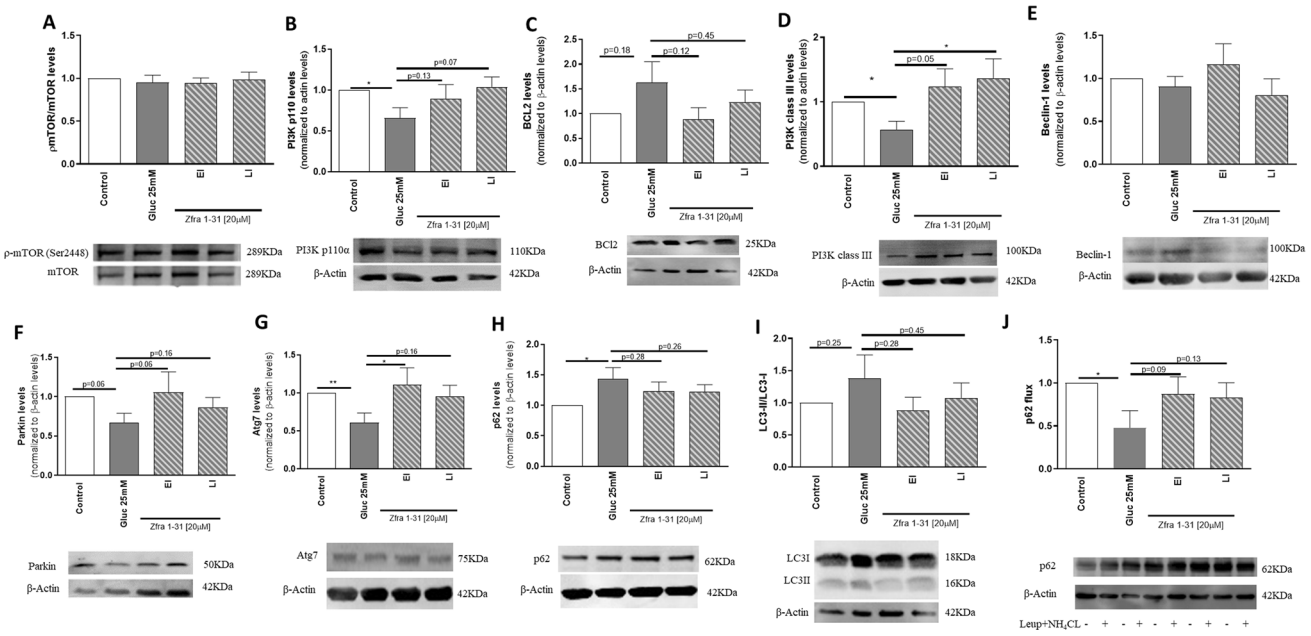

Fig. 8 ρWWOX (tyr33) inhibition by Zfra1-31 restores autophagy. **A** ρmTOR/mTOR levels and representative Western blot image; **B** PI3K p110 levels and representative Western blot image; **C** BCL2 levels and representative Western blot image; **D** PI3K class III levels and representative Western blot image; **E** Beclin 1 levels and representative Western blot image; **F** Parkin levels and representative Western blot image; **G** Atg 7 levels and representative Western blot image; **H** p62 levels and representative Western blot image; **I** LC3-II levels and representative Western blot image; **J** p62 flux levels and representative Western blot image. Data shown represent mean ± SEM from 4/6 independent experiments. Statistical significance: $*p < 0.05$; $**p < 0.01$ when compared with respective condition. *WWOX* putative tumor suppressor WW domain-containing oxidoreductase 1, *EI* early intervention, *LI* late intervention, *mTOR* mammalian target of rapamycin, *PI3K* phosphoinositide 3-kinase, *BCL2* B-cell lymphoma 2, *Atg7* autophagy related 7, *LC3* microtubule-associated protein 1A/1B-light chain 3

In particular, a moderate increase in B-cell lymphoma 2 (BCL2) (Fig. 8C), a significant decrease (~43%) in PI3K class III, and a non-statistically significant decrease in Parkin levels (Fig. 8D, F) were observed in cells exposed to high glucose. In relation to Beclin levels, no significant alterations were observed in cells exposed to high glucose (Fig. 8E). Together, these observations suggest that the initiation complex is not being properly assembled. The following steps of the autophagic process were also compromised by high glucose as shown by a decrease (~39%) in autophagy related 7 (Atg7) and a significant increase (~58%) in p62 levels (Fig. 8G, H) suggesting an impairment of the elongation phase of autophagy. More, high glucose significantly decreased (~52%) the autophagic p62 flux (Fig. 8J) leading to an increase (~38%) in the accumulation of microtubule-associated protein 1A/1B-light chain 3 (LC3)-II (Fig. 8I). Interestingly, Zfra 1–31, in EI condition, significantly increased (~50%) Atg7 levels and, in the LI condition, it significantly increased (~79%) PI3K class III levels (Fig. 8D, G). Zfra1-31 tended to normalize the levels of the other proteins analyzed (Fig. 8A–J). Altogether these observations suggest that Zfra1-31 is capable of partially restoring the autophagic process.

The inhibition of WWOX activation by Zfra1-31 avoids the increase in the levels of neurotoxic proteins and the loss of synapse integrity under high glucose conditions

It has been previously reported that hyperglycemia/diabetes increases the risk of dementia, particularly vascular dementia and AD, due to several cellular and molecular alterations including the increase in the levels of neurotoxic proteins namely phosphorylated Tau (pTau) and amyloid β (Aβ) proteins [4]. In our experimental conditions, high glucose promoted a twofold increase in pTau (ser396) and a threefold increase in Aβ levels (Fig. 9D, E). Interestingly, Zfra1-31 was able to normalize Aβ protein levels by causing a ~60% decrease in the EI condition and a ~58% decrease in LI condition (Fig. 9D, E). Zfra1-31 also promoted a ~73% and a ~52% decrease in the pTau (ser396) protein levels in EI and LI conditions, respectively, supporting the therapeutic effectiveness of Zfra1-31 against hyperglycemia/diabetes-induced neurodegeneration.

Knowing that neuronal cells are highly reliant on mitochondria and sensitive to stress, alterations in cell and mitochondrial homeostasis will have a profound impact on cells' integrity and function. To evaluate synaptic integrity, we

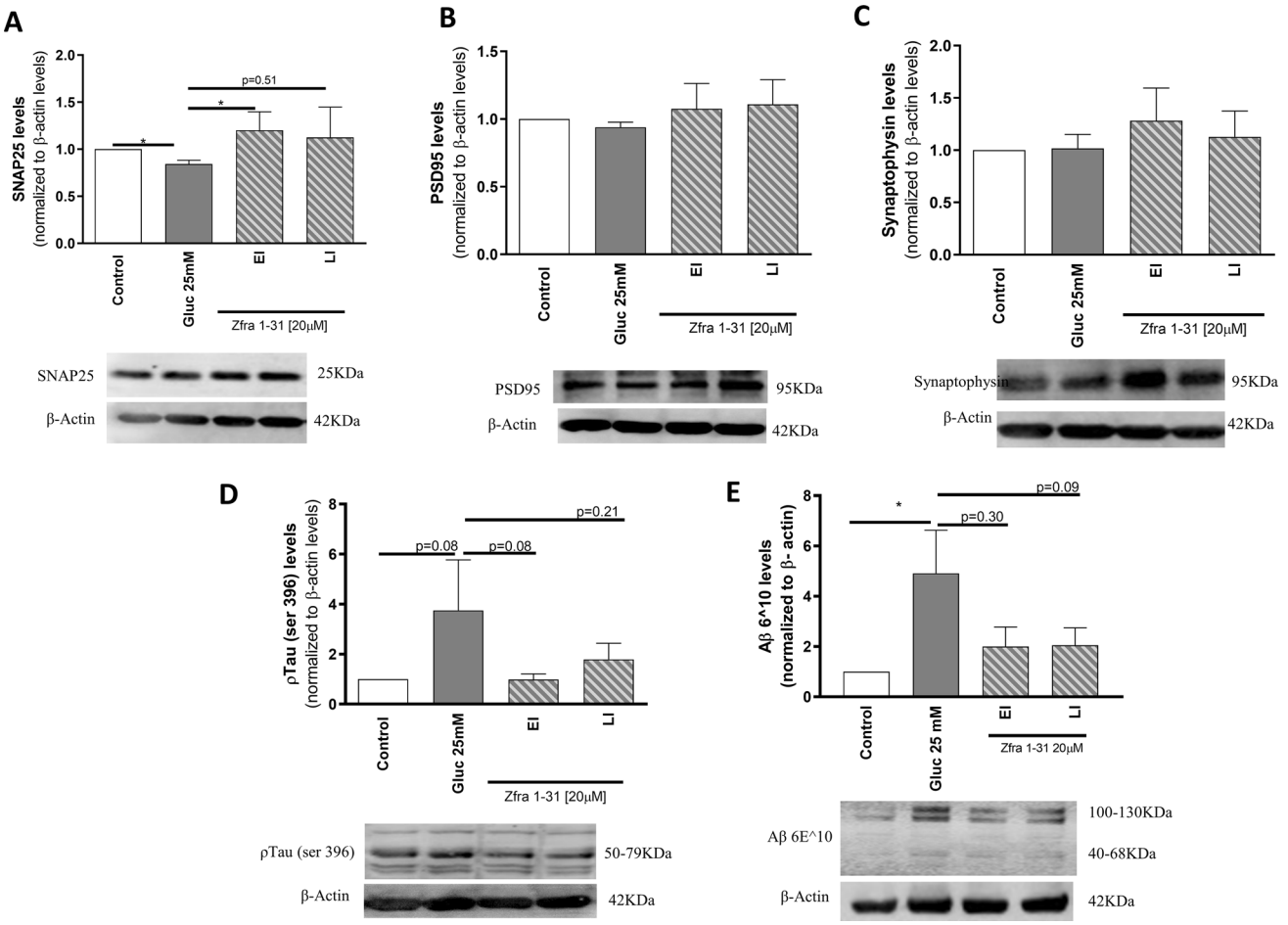

Fig. 9 ρWWOX (tyr33) inhibition by Zfra1-31 reduces the levels of neurotoxic proteins and increases synaptic integrity. **A** SNAP25 levels and representative western blot image; **B** PSD95 levels and representative western blot image; **C** synaptophysin levels and representative western blot image; **D** ptau protein levels and representative Western blot image; **E** Aβ protein and representative Western blot image. Data shown represent mean ± SEM from 4/6 independent experiments. Statistical significance: $*p < 0.05$ when compared with respective condition. *WWOX* putative tumor suppressor WW domain-containing oxidoreductase 1, *EI* early intervention, *LI* late intervention, *SNAP25* synaptosomal-associated protein, 25 kDa, *PSD95* postsynaptic density protein 95, *ptau* phosphorylated tau protein, *Aβ* amyloid β protein

measured the levels of the presynaptic proteins synaptosomal-associated protein, 25 kDa (SNAP25) and synaptophysin and the postsynaptic protein postsynaptic density protein 95 (PSD95). High glucose caused a significant decrease (~20%) in the levels of SNAP25 (Fig. 9A) and did not alter significantly PSD95 or synaptophysin levels (Fig. 9B, C). Zfra1-31, in both EI and LI conditions (Fig. 9A) tended to normalize the levels of these proteins suggesting that Zfra1-31 contributes to the maintenance of synaptic integrity.

Discussion

In this study we show for the first time that WWOX activation, through tyrosine 33 residue phosphorylation, is an early event in diabetic/hyperglycemic conditions and its activation is closely associated with mitochondrial and cellular dyshomeostasis. More, we demonstrate that the inhibition of WWOX activation by its specific inhibitor Zfra1-31 reverses diabetes/hyperglycemia-associated deleterious effects in mitochondria and neuronal cells. These observations support the involvement of WWOX in neurodegeneration-associated to diabetes and the therapeutic potential of Zfra1-31 in this complication (Fig. 10).

The literature clearly shows that mitochondrial dysfunction is a strong player in the connection between diabetes-associated neuronal/brain defects and neurodegenerative disorders [4, 9–11, 35, 41, 42]. However, the mechanisms underlying this connection are not fully elucidated. As previously described, the brain requires a constant supply of energy to maintain normal neuronal and synaptic activities [43, 44]. In neuronal cells mitochondria are the main source

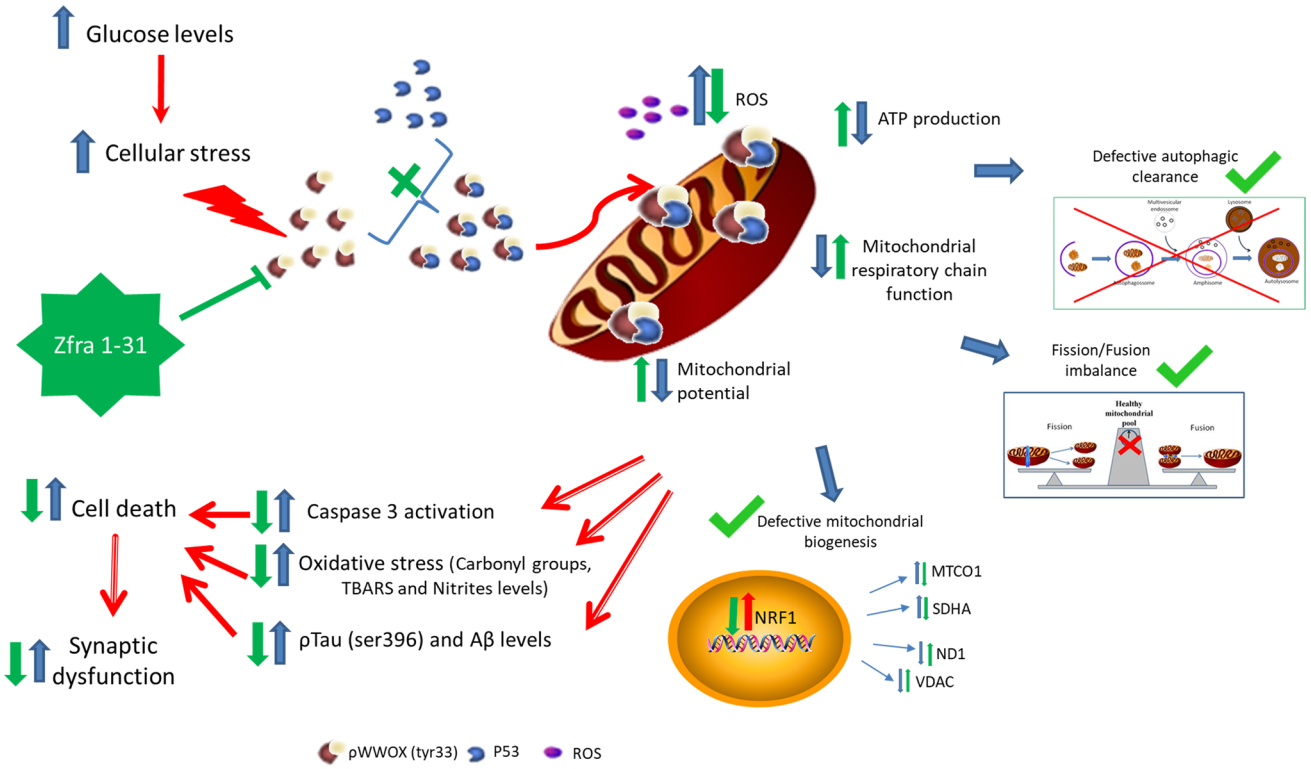

Fig. 10 Proposed mechanism of action. High glucose increases cellular stress activating WWOX through the phosphorylation of tyrosine 33 residue. Phosphorylated WWOX can bind to p53 in the cytosol and the complex can migrate to mitochondria decreasing their function, increasing ROS production and oxidative damage and leading to an energy crisis. Moreover, increased activation of WWOX (tyr33 phosphorylation) also seems to interfere with cell and mitochondrial quality control mechanisms leading to an accumulation of damaged mitochondria and neurotoxic proteins. Together, such alterations are responsible for the loss of synaptic integrity and cell death. Zfra1-31, by inhibiting WWOX can recover mitochondria and cellular homeostasis promoting neuronal viability and integrity. *WWOX* putative tumor suppressor WW domain-containing oxidoreductase 1, *ROS* reactive oxygen species, *MTCO1* mitochondrially encoded cytochrome C oxidase I, *ND1* NADH-ubiquinone oxidoreductase chain 1, *VDAC* voltage-dependent anion channel, *SDHA* succinate dehydrogenase complex flavoprotein subunit A, *NRF1* nuclear respiratory factor 1, $\Delta\Psi m$ mitochondrial membrane potential

of energy so, alterations in these organelles will severely impact neurons, compromising cognitive function [45, 46]. Although the involvement of WWOX in brain development and pathology was already described [45], scarce evidence exists concerning the interaction between WWOX and mitochondria in brain cells.

Using brain cortical and hippocampal homogenates, we observed that young animals (6-month-old) present increased levels of pWWOX (tyr33), when compared to age-matched control rats and to 12-month-old GK rats (Fig. 2A, B). This observation is very interesting since we have previously demonstrated that brain cortical mitochondria from 6-month-old GK rats are preserved [10] while those from 12-month-old GK rats are dysfunctional [46]. Others also showed that liver mitochondria from 6-month-old GK rats function is slightly better than liver mitochondria from control rats, which may result from compensatory mechanisms [36]. Altogether, this evidence suggests that pWWOX (tyr33) precedes mitochondrial dysfunction. Accordingly, our in vitro studies revealed an increase in pWWOX (tyr33) levels 24 h after high glucose (25 mM) exposure while mitochondrial dysfunction and subsequent cell death were observed only at 48 h after high glucose exposure (Fig. 2C, D). A study performed in a mouse model of AD showed that WWOX is involved in the development of the pathology [15]. Another study performed in MPP^+ rat brains, a model of PD, showed increased levels of pWWOX (tyr33) in the injured neurons of the striatum and cortex, being this protein localized in damaged mitochondria of degenerative neurons [18]. Furthermore, it was observed that pWWOX decreased 1–2 months after injury [18], which is in accordance with our observations. It was also previously reported that under cellular stress WWOX undergoes tyrosine 33 residue phosphorylation [47]. However, with aging a shift between phosphorylated residues occurs; tyrosine 33 residue phosphorylation decreases and serine 14 residue phosphorylation increases, which seems to contribute to neuronal degeneration [48]. It was also shown that the complete loss of WWOX protein due to alterations in its gene (missense or nonsense mutations and deletions) can

lead to the development of neural disorders and metabolic diseases including ataxia, epilepsy, dementia, neurodegeneration, growth retardation, abnormal high density lipoproteins (HDL) metabolism, and early death [22, 49]. Here we present evidence that increased activation of WWOX also plays a role in neuronal degeneration and death under hyperglycemic/diabetic conditions.

Previous studies from our laboratory show a close association between T2D and AD. Using mouse models of the two diseases we observed that these two pathological conditions share several mechanisms, including defects in mitochondria and redox imbalance, which culminate in synaptic alterations and cognitive defects [4, 13]. Using a rat model of T1D, we also demonstrated that mitochondrial dysfunction and oxidative stress play a key role in brain damage [8, 9, 14]. Since we observed that enhanced WWOX activation is involved in mitochondrial dysfunction and brain/neuronal damage under diabetic/hyperglycemic conditions (Figs. 4, 9), we hypothesized that Zfra1-31 is a potential therapeutic agent for diabetes-associated neurodegeneration. Accordingly, we observed that Zfra1-31 was capable of reverting pWWOX (tyr33)-mediated mitochondrial dysfunction and cell death (Fig. 4A, 3B).

It has been widely described that hyperglycemia is responsible for mitochondrial dysfunction, increased ROS production and oxidative stress/damage [50], as observed in this study (Figs. 4, 5). Importantly, our study shows that the inhibition of WWOX under high glucose conditions can revert mitochondrial dysfunction (Fig. 4), including their capacity to produce ATP (Fig. 4F, H) and oxidative damage (Fig. 5). pWWOX (tyr33) under stress conditions interacts with p53 forming a protein complex that migrates to mitochondria activating the pro-apoptotic pathway [16]. Accordingly, increased p53 protein levels and caspase 3 activity were observed in cells exposed to high glucose (Fig. 3C, D), which contributes to mitochondrial dysfunction and oxidative stress/damage (Figs. 4, 5). Moreover, it was previously shown that inhibition of tyr33 phosphorylation by a dominant-negative WWOX was able to abolish apoptotic cell death in a MPP^+ rat model for PD, indicating a critical role of WWOX phosphorylation in apoptosis [18]. p53 has been shown to play a pivotal role in evoking apoptotic cell death in conditions of genotoxic stress as an attempt to maintain cellular integrity [51]. p53 can also act as a repressor of autophagy in different cell types [51] and mitophagy (the selective mitochondrial engulfment and digestion by autophagy) is compromised in brain tissue from diabetic animals as well as in neuronal cells exposed to high glucose [35, 52, 53]. We have previously reported the existence of alterations in autophagy in T2D animal models [10, 11, 35, 54]. And, anomalies in autophagy have been associated with the accumulation of mutant/misfolded and aggregated proteins and dysfunctional organelles within cells, which occur in several pathologies including neurodegenerative diseases [55]. In the present study we also observed an altered autophagic process in neuronal cells exposed to high glucose (Fig. 8). In more detail, high glucose decreased the levels of key executer proteins of the autophagic process namely PI3K p110 (insulin-dependent autophagy regulation), PI3K class III and Atg7 as well as p62 flux (Fig. 8). And, the inhibition of WWOX by Zfra1-31 partially restored this process (Fig. 8). Although we did not observe alterations in mTOR activation (Fig. 8A), one of the main autophagic regulators in the initiation phase of the process, it is important to mention that mTOR activation can also occur through the phosphorylation of one of three residues and, in this case, only serine 2448 residue (the most analyzed residue) was evaluated, So, we cannot exclude possible alterations in other residues. Defects in cell quality control mechanisms can also be responsible for the accumulation of neurotoxic proteins such as Aβ and pTau proteins, as observed in our study (Fig. 9D, E). In accordance with our observations, previous in vivo/ex vivo studies demonstrated that diabetes increases the levels of Aβ and pTau proteins [4, 5, 56–59]. Zfra1-31 was able to reduce the levels of these neurotoxic proteins (Fig. 9D, E), as previously demonstrated in a mouse model of AD [20].

The coordination of mitochondrial fission/fusion processes lowers the amount of defective mitochondria and ensures cell homeostasis [60] whereas the occurrence of mitochondrial dynamics distortion (excessive fragmentation or fusion) results in cells functioning anomalies and, eventually, death [61]. In our study, the imbalance of mitochondrial fission/fusion-related proteins occurred in neuronal cells exposed to high glucose, characterized by an increase in protein levels of Fis1 and OPA-1 and a decrease in Mfn1 and pDRP1/DRP1 (Fig. 6). DRP1 is considered the main mediator of mitochondrial fission and Fis1 is one of its main mitochondrial receptors, which recruits DRP1 to mitochondrial membranes where it assembles into a ring-like structure to constrict the membranes [55]. Mitochondrial morphology results from a strict balance between fission and fusion [62] and is considered a major process for adaptation of mitochondrial bioenergetic efficiency and energy substrates oxidation regulating cellular metabolism and fine-tuning energy levels [55]. Interestingly, here we show that WWOX inhibition by Zfra1-31 tended to reestablish fission/fusion balance (Fig. 6) under hyperglycemic conditions.

It is far known that cells respond to different physiological, metabolic, and pathological changes by regulating mitochondrial morphology and function; being mitochondrial biogenesis one of the processes involved in this regulation [63]. The fine-tuning from protein synthesis to the nascent assembly of OXPHOS complexes requires strict regulatory mechanisms that coordinate mitochondrial translation to ensure correct and efficient synthesis, transport, localization,

and assembly of the mitochondrial complexes [64]. Here we observed that the increased protein levels of NRF1, MTCO1 and SDHA (Fig. 7A, D, E) under high glucose conditions was not accompanied by increased levels of other mitochondrial proteins (Fig. 7B, C) suggesting a defective mitochondrial assembly. It was previously reported that under high glucose conditions, mitochondria undergo biogenesis however, the increased biogenesis is insufficient to accommodate the metabolic load, which exacerbates mitochondrial fission resulting in smaller and damaged mitochondria [39]. Accordingly, we observed that the imbalance in mitochondria biogenesis is associated with other mitochondrial anomalies affecting their function. Again, the inhibition of WWOX by Zfra1-31 partially recovered high glucose-induced mitochondrial biogenesis anomalies (Fig. 7).

Because the integrity of synapses is crucial to maintain normal function of neuronal cells, we evaluated the levels of some markers of synaptic integrity. High glucose caused a decrease in the presynaptic marker SNAP25 protein levels but did not significantly alter the levels of the postsynaptic marker PSD95 and the presynaptic marker synaptophysin (Fig. 9). It is known that SNAP25 participates in docking and/or fusion of synaptic vesicles with the plasmalemma, a process essential for synaptic vesicle exocytosis [65]. PSD95 seems to be involved in synapse maturation wielding a major influence on synaptic strength and plasticity [66]. Concerning synaptophysin, its function remains uncertain, although it seems to be necessary for kinetically efficient endocytosis of synaptic vesicles in neurons [67]. So, our observations suggest that high glucose interferes with synaptic integrity by decreasing vesicle exocytosis. These results are in agreement with previous studies showing a decrease in SNAP25 protein levels without significant changes in PSD95 or synaptophysin protein levels in brain samples from T1D and T2D animal models [9, 35]. Neuronal cells exposed to high glucose and treated with Zfra1-31 show normalized SNAP25 protein levels and a slight increase in both PSD95 and synaptophysin protein levels suggesting that Zfra1-31 improves synaptic function and possibly ameliorates learning and memory, which are impaired under diabetic conditions [13].

Conclusions

In sum, our results show that WWOX activation through tyr33 phosphorylation occurs prior to mitochondrial dysfunction and cell death suggesting that hyperglycemia-induced neuronal damage and death involves WWOX-mediated mitochondrial dysfunction and apoptosis activation. Moreover, we showed that pWWOX (tyr33) inhibition by Zfra1-31 peptide ameliorates hyperglycemia-associated neurodegeneration by acting upstream mitochondrial dysfunction. There is an increased realization by the pharmaceutical industry that every drug design for the treatment of diverse pathologies must be tested at an early stage for adverse effects on mitochondria [65] to obtain the most physiologically relevant, unambiguous and informative results [66]. Our observations revealed that Zfra1-31, besides being effective against high glucose-induced mitochondrial defects, does not affect mitochondria and cells function under control conditions (data not shown). So, we believe that WWOX is a new therapeutic target to have in consideration in diabetes-associated neurodegeneration and that Zfra1-31 is a possible therapeutic agent to treat this complication.

In vitro studies have several advantages such as the tight control of cells' environment, reduced costs, and high throughput. However, a major weakness of the in vitro studies is that they fail to replicate the conditions of the cells in an organism including the crosstalk that exists between the various cell types. Although our study presents robust data supporting the therapeutic potential of Zfra1-31, the efficacy of the compound must be assessed in vivo which will allow to understand how Zfra1-31 modulates peripheral and central metabolism and cognitive function, among other things. Future studies must also focus on specific regions of the brain (e.g., specific brain cortical areas and *substantia nigra*) to identify which brain regions are more susceptible to WWOX-mediated neurodegenerative events. Due to the limited amount of rat brain samples, we were unable to perform key experiments done in neuronal cells such as the evaluation of the levels of neurotoxic proteins and synaptic integrity markers. Nevertheless, previous studies from our laboratory and others demonstrated that GK rats present AD-like features including an increase in pTau and Aβ protein levels and cognitive dysfunction [5, 56–59].

Supplementary Information The online version contains supplementary material available at https://doi.org/10.1007/s00018-022-04508-7.

Author contributions All authors contributed to the study conception and design and results interpretation. Material preparation, data collection and analysis were performed by CC. Cells acquisition and preparation were made by SC. RS was responsible for GK and Wistar control rats colonies maintenance and breeding. The first draft of the manuscript was written by CC. PM helped in the experimental design, results discussion and revised the manuscript.

Funding The authors' work is supported by the European Regional Development Fund (ERDF), through the Centro 2020 Regional Operational Programme, the COMPETE 2020—Operational Programme for Competitiveness and Healthy Aging 2020 (CENTRO-01-0145-FEDER-000012) and national funds from FCT—Foundation for Science and Technology under the project PEst-C/SAU/LA0001/2013-2014; EXPL/MED-FSL/0033/2021 and strategic

projects UIDB/04539/2020; UIDP/04539/2020 and LA/P/0058/2020". Cristina Carvalho has a work contract under the Individual Call to Scientific Employment Stimulus—1st Edition (CEECIND/02201/2017).

Data availability The datasets generated during and/or analyzed during the current study are available from the corresponding author on reasonable request.

Declarations

Conflict of interest The authors have no relevant financial or non-financial interests to disclose.

References

1. Brussels, Belgium. 2021. https://www.diabetesatlas.org. Accessed 10 Feb 2022
2. International Diabetes Federation I (2019) IDF Diabetes Atlas, 9th edn. Brussels. https://www.diabetesatlas.org. Accessed 2020
3. Correia S, Carvalho C, Santos R, Cardoso S, Santos M, Moreira P (2010) Diabetes as a trigger of neurodegeneration: from pathophysiological mechanisms to therapeutic approaches. In: Stefek M (ed) Advances in molecular mechanisms and pharmacology of diabetic complications, pp 175–198
4. Carvalho C, Cardoso S, Correia SC, Santos RX, Santos MS, Baldeiras I et al (2012) Metabolic alterations induced by sucrose intake and Alzheimer's disease promote similar brain mitochondrial abnormalities. Diabetes 61(5):1234–1242. https://doi.org/10.2337/db11-1186
5. Candeias E, Duarte AI, Sebastiao I, Fernandes MA, Placido AI, Carvalho C et al (2017) Middle-aged diabetic females and males present distinct susceptibility to Alzheimer disease-like pathology. Mol Neurobiol 54(8):6471–6489. https://doi.org/10.1007/s12035-016-0155-1
6. Carvalho CPIM (2020) Cognitive impairment in obesity and diabetes. In: Faintuch JSF (ed) Obesity and diabetes. Springer, Berlin
7. Sun Y, Ma C, Sun H, Wang H, Peng W, Zhou Z et al (2020) Metabolism: a novel shared link between diabetes mellitus and Alzheimer's disease. J Diabetes Res 2020:4981814. https://doi.org/10.1155/2020/4981814
8. Cardoso S, Santos MS, Seica R, Moreira PI (2010) Cortical and hippocampal mitochondria bioenergetics and oxidative status during hyperglycemia and/or insulin-induced hypoglycemia. Biochim Biophys Acta 1802(11):942–951. https://doi.org/10.1016/j.bbadis.2010.07.001
9. Cardoso S, Santos RX, Correia SC, Carvalho C, Santos MS, Baldeiras I et al (2012) Insulin-induced recurrent hypoglycemia exacerbates diabetic brain mitochondrial dysfunction and oxidative imbalance. Neurobiol Dis 49C:1–12. https://doi.org/10.1016/j.nbd.2012.08.008
10. Santos RX, Correia SC, Alves MG, Oliveira PF, Cardoso S, Carvalho C et al (2014) Mitochondrial quality control systems sustain brain mitochondrial bioenergetics in early stages of type 2 diabetes. Mol Cell Biochem 394(1–2):13–22. https://doi.org/10.1007/s11010-014-2076-5
11. Santos RX, Correia SC, Alves MG, Oliveira PF, Cardoso S, Carvalho C et al (2014) Insulin therapy modulates mitochondrial dynamics and biogenesis, autophagy and tau protein phosphorylation in the brain of type 1 diabetic rats. Biochim Biophys Acta 1842(7):1154–1166. https://doi.org/10.1016/j.bbadis.2014.04.011
12. Rocha M, Apostolova N, Diaz-Rua R, Muntane J, Victor VM (2020) Mitochondria and T2D: role of autophagy, ER stress, and inflammasome. Trends Endocrinol Metab 31(10):725–741. https://doi.org/10.1016/j.tem.2020.03.004
13. Carvalho C, Machado N, Mota P, Correia S, Cardoso S, Santos R et al (2013) Type 2 diabetic and Alzheimer's disease mice present similar behavioral, cognitive and vascular anomalies. J Alzheimer Dis 35(3)
14. Cardoso S, Seica RM, Moreira PI (2018) Uncoupling protein 2 inhibition exacerbates glucose fluctuation-mediated neuronal effects. Neurotox Res 33(2):388–401. https://doi.org/10.1007/s12640-017-9805-y
15. Teng CC, Yang YT, Chen YC, Kuo YM, Sze CI (2012) Role of WWOX/WOX1 in Alzheimer's disease pathology and in cell death signaling. Front Biosci (Elite Ed) 4:1951–1965
16. Chang NS, Doherty J, Ensign A, Lewis J, Heath J, Schultz L et al (2003) Molecular mechanisms underlying WOX1 activation during apoptotic and stress responses. Biochem Pharmacol 66(8):1347–1354 (**S0006295203004842 [pii]**)
17. Sze CI, Su M, Pugazhenthi S, Jambal P, Hsu LJ, Heath J et al (2004) Down-regulation of WW domain-containing oxidoreductase induces Tau phosphorylation in vitro. A potential role in Alzheimer's disease. J Biol Chem 279(29):30498–30506. https://doi.org/10.1074/jbc.M401399200
18. Lo CP, Hsu LJ, Li MY, Hsu SY, Chuang JI, Tsai MS et al (2008) MPP+-induced neuronal death in rats involves tyrosine 33 phosphorylation of WW domain-containing oxidoreductase WOX1. Eur J Neurosci 27(7):1634–1646. https://doi.org/10.1111/j.1460-9568.2008.06139.x
19. Tabarki B, AlHashem A, AlShahwan S, Alkuraya FS, Gedela S, Zuccoli G (2015) Severe CNS involvement in WWOX mutations: description of five new cases. Am J Med Genet A 167A(12):3209–3213. https://doi.org/10.1002/ajmg.a.37363
20. Lee MH, Shih YH, Lin SR, Chang JY, Lin YH, Sze CI et al (2017) Zfra restores memory deficits in Alzheimer's disease triple-transgenic mice by blocking aggregation of TRAPPC6ADelta, SH3GLB2, tau, and amyloid beta, and inflammatory NF-kappaB activation. Alzheimers Dement 3(2):189–204. https://doi.org/10.1016/j.trci.2017.02.001
21. Huang SS, Chang NS (2018) Phosphorylation/de-phosphorylation in specific sites of tumor suppressor WWOX and control of distinct biological events. Exp Biol Med (Maywood) 243(2):137–147. https://doi.org/10.1177/1535370217752350
22. Chang HT, Liu CC, Chen ST, Yap YV, Chang NS, Sze CI (2014) WW domain-containing oxidoreductase in neuronal injury and neurological diseases. Oncotarget 5(23):11792–11799. https://doi.org/10.18632/oncotarget.2961
23. Suzuki H, Katayama K, Takenaka M, Amakasu K, Saito K, Suzuki K (2009) A spontaneous mutation of the Wwox gene and audiogenic seizures in rats with lethal dwarfism and epilepsy. Genes Brain Behav 8(7):650–660. https://doi.org/10.1111/j.1601-183X.2009.00502.x
24. Mallaret M, Synofzik M, Lee J, Sagum CA, Mahajnah M, Sharkia R et al (2014) The tumour suppressor gene WWOX is mutated in autosomal recessive cerebellar ataxia with epilepsy and mental retardation. Brain 137(Pt 2):411–419. https://doi.org/10.1093/brain/awt338
25. Elsaadany L, El-Said M, Ali R, Kamel H, Ben-Omran T (2016) W44X mutation in the WWOX gene causes intractable seizures and developmental delay: a case report. BMC Med Genet 17(1):53. https://doi.org/10.1186/s12881-016-0317-z
26. Silva DF, Esteves AR, Oliveira CR, Cardoso SM (2017) Mitochondrial metabolism power SIRT2-dependent deficient traffic causing Alzheimer's-disease related pathology. Mol Neurobiol 54(6):4021–4040. https://doi.org/10.1007/s12035-016-9951-x

27. Riss TL, Moravec RA, Niles AL, Duellman S, Benink HA, Worzella TJ et al (2004) Cell viability assays. In: Sittampalam GS, Coussens NP, Brimacombe K, Grossman A, Arkin M, Auld D et al (eds) Assay guidance manual. Bethesda (MD)
28. Scaduto RC Jr, Grotyohann LW (1999) Measurement of mitochondrial membrane potential using fluorescent rhodamine derivatives. Biophys J 76(1 Pt 1):469–477. https://doi.org/10.1016/S0006-3495(99)77214-0
29. Dickinson BC, Lin VS, Chang CJ (2013) Preparation and use of MitoPY1 for imaging hydrogen peroxide in mitochondria of live cells. Nat Protoc 8(6):1249–1259. https://doi.org/10.1038/nprot.2013.064
30. Colombo G, Clerici M, Garavaglia ME, Giustarini D, Rossi R, Milzani A et al (2016) A step-by-step protocol for assaying protein carbonylation in biological samples. J Chromatogr B Anal Technol Biomed Life Sci 1019:178–190. https://doi.org/10.1016/j.jchromb.2015.11.052
31. Green LC, Ruiz de Luzuriaga K, Wagner DA, Rand W, Istfan N, Young VR et al (1981) Nitrate biosynthesis in man. Proc Natl Acad Sci USA 78(12):7764–7768. https://doi.org/10.1073/pnas.78.12.7764
32. Ernster L, Nordenbrand K (1967) Microsomal lipid peroxidation. Methods Enzymol 10:574–580
33. Silva DF, Selfridge JE, Lu J, Roy N, Hutfles L et al (2013) Bioenergetic flux, mitochondrial mass and mitochondrial morphology dynamics in AD and MCI cybrid cell lines. Hum Mol Genet 22(19):3931–3946. https://doi.org/10.1093/hmg/ddt247
34. Esteves AR, Arduino DM, Silva DF, Viana SD, Pereira FC, Cardoso SM (2018) Mitochondrial metabolism regulates microtubule acetylome and autophagy trough sirtuin-2: impact for Parkinson's disease. Mol Neurobiol 55(2):1440–1462. https://doi.org/10.1007/s12035-017-0420-y
35. Carvalho C, Santos MS, Oliveira CR, Moreira PI (2015) Alzheimer's disease and type 2 diabetes-related alterations in brain mitochondria, autophagy and synaptic markers. Biochim Biophys Acta 1852(8):1665–1675. https://doi.org/10.1016/j.bbadis.2015.05.001
36. Ferreira FM, Palmeira CM, Seica R, Moreno AJ, Santos MS (2003) Diabetes and mitochondrial bioenergetics: alterations with age. J Biochem Mol Toxicol 17(4):214–222. https://doi.org/10.1002/jbt.10081
37. Dalle-Donne I, Rossi R, Giustarini D, Milzani A, Colombo R (2003) Protein carbonyl groups as biomarkers of oxidative stress. Clin Chimica Acta 329(1–2):23–38. https://doi.org/10.1016/s0009-8981(03)00003-2
38. Babbar M, Sheikh MS (2013) Metabolic stress and disorders related to alterations in mitochondrial fission or fusion. Mol Cell Pharmacol 5(3):109–133
39. Edwards JL, Quattrini A, Lentz SI, Figueroa-Romero C, Cerri F, Backus C et al (2010) Diabetes regulates mitochondrial biogenesis and fission in mouse neurons. Diabetologia 53(1):160–169. https://doi.org/10.1007/s00125-009-1553-y
40. Shen X, Zheng S, Thongboonkerd V, Xu M, Pierce WM Jr, Klein JB et al (2004) Cardiac mitochondrial damage and biogenesis in a chronic model of type 1 diabetes. Am J Physiol Endocrinol Metab 287(5):E896-905. https://doi.org/10.1152/ajpendo.00047.2004
41. Cardoso SM, Correia SC, Carvalho C, Moreira PI (2017) Mitochondria in Alzheimer's disease and diabetes-associated neurodegeneration: license to heal! Handb Exp Pharmacol 240:281–308. https://doi.org/10.1007/164_2017_3
42. Huang YC, Hsu SM, Shie FS, Shiao YJ, Chao LJ, Chen HW et al (2022) Reduced mitochondria membrane potential and lysosomal acidification are associated with decreased oligomeric Abeta degradation induced by hyperglycemia: a study of mixed glia cultures. PLoS ONE 17(1):e0260966. https://doi.org/10.1371/journal.pone.0260966
43. Moreira PI (2018) Sweet mitochondria: a shortcut to Alzheimer's disease. J Alzheimer's Dis 62(3):1391–1401. https://doi.org/10.3233/JAD-170931
44. Cunnane SC, Trushina E, Morland C, Prigione A, Casadesus G, Andrews ZB et al (2020) Brain energy rescue: an emerging therapeutic concept for neurodegenerative disorders of ageing. Nat Rev Drug Discov 19(9):609–633. https://doi.org/10.1038/s41573-020-0072-x
45. Kosla K, Kaluzinska Z, Bednarek AK (2020) The WWOX gene in brain development and pathology. Exp Biol Med (Maywood) 245(13):1122–1129. https://doi.org/10.1177/1535370220924618
46. Moreira PI, Santos MS, Moreno AM, Seica R, Oliveira CR (2003) Increased vulnerability of brain mitochondria in diabetic (Goto-Kakizaki) rats with aging and amyloid-beta exposure. Diabetes 52(6):1449–1456
47. Chang NS, Hsu LJ, Lin YS, Lai FJ, Sheu HM (2007) WW domain-containing oxidoreductase: a candidate tumor suppressor. Trends Mol Med 13(1):12–22. https://doi.org/10.1016/j.molmed.2006.11.006
48. Hsu CY, Lee KT, Sun TY, Sze CI, Huang SS, Hsu LJ et al (2021) WWOX and its binding proteins in neurodegeneration. Cells. https://doi.org/10.3390/cells10071781
49. Abdel-Salam G, Thoenes M, Afifi HH, Körber F, Swan D, Bolz HJ (2014) The supposed tumor suppressor gene WWOX is mutated in an early lethal microcephaly syndrome with epilepsy, growth retardation and retinal degeneration. Orphanet J Rare Dis 9(1):12. https://doi.org/10.1186/1750-1172-9-12
50. Palmeira CM, Rolo AP, Berthiaume J, Bjork JA, Wallace KB (2007) Hyperglycemia decreases mitochondrial function: the regulatory role of mitochondrial biogenesis. Toxicol Appl Pharmacol 225(2):214–220. https://doi.org/10.1016/j.taap.2007.07.015
51. Salminen A, Kaarniranta K (2009) SIRT1: regulation of longevity via autophagy. Cell Signal 21(9):1356–1360. https://doi.org/10.1016/j.cellsig.2009.02.014
52. Miao Y, Guo D, Li W, Zhong Y (2019) Diabetes promotes development of Alzheimer's disease through suppression of autophagy. J Alzheimer's Dis 69(1):289–296. https://doi.org/10.3233/JAD-190156
53. Ni HM, Williams JA, Ding WX (2015) Mitochondrial dynamics and mitochondrial quality control. Redox Biol 4:6–13. https://doi.org/10.1016/j.redox.2014.11.006
54. Santos RX, Correia SC, Wang X, Perry G, Smith MA, Moreira PI et al (2010) A synergistic dysfunction of mitochondrial fission/fusion dynamics and mitophagy in Alzheimer's disease. J Alzheimer's Dis 20(Suppl 2):S401–S412. https://doi.org/10.3233/JAD-2010-100666
55. Luo L, Qin ZH (2019) Autophagy, aging, and longevity. Adv Exp Med Biol 1206:509–525. https://doi.org/10.1007/978-981-15-0602-4_24
56. Hussain S, Mansouri S, Sjoholm A, Patrone C, Darsalia V (2014) Evidence for cortical neuronal loss in male type 2 diabetic Goto-Kakizaki rats. J Alzheimer's Dis 41(2):551–560. https://doi.org/10.3233/JAD-131958
57. Pintana H, Apaijai N, Kerdphoo S, Pratchayasakul W, Sripetchwandee J, Suntornsaratoon P et al (2017) Hyperglycemia induced the Alzheimer's proteins and promoted loss of synaptic proteins in advanced-age female Goto-Kakizaki (GK) rats. Neurosci Lett 655:41–45. https://doi.org/10.1016/j.neulet.2017.06.041
58. Movassat J, Delangre E, Liu J, Gu Y, Janel N (2019) Hypothesis and theory: circulating Alzheimer's-related biomarkers in type 2 diabetes insight from the Goto-Kakizaki Rat. Front Neurol 10:649. https://doi.org/10.3389/fneur.2019.00649

59. Ke B, Zhang T, An T, Lu R (2020) Soy isoflavones ameliorate the cognitive dysfunction of Goto-Kakizaki rats by activating the Nrf2-HO-1 signalling pathway. Aging (Albany NY) 12(21):21344–21354. https://doi.org/10.18632/aging.103877
60. Dai W, Jiang L (2019) Dysregulated mitochondrial dynamics and metabolism in obesity, diabetes, and cancer. Front Endocrinol (Lausanne) 10:570. https://doi.org/10.3389/fendo.2019.00570
61. Sprenger HG, Langer T (2019) The good and the bad of mitochondrial breakups. Trends Cell Biol 29(11):888–900. https://doi.org/10.1016/j.tcb.2019.08.003
62. Scott I, Youle RJ (2010) Mitochondrial fission and fusion. Essays Biochem 47:85–98. https://doi.org/10.1042/bse0470085
63. Sanchis-Gomar F, Garcia-Gimenez JL, Gomez-Cabrera MC, Pallardo FV (2014) Mitochondrial biogenesis in health and disease. Molecular and therapeutic approaches. Curr Pharm Des 20(35):5619–5633. https://doi.org/10.2174/1381612820666140306095106
64. Tang JX, Thompson K, Taylor RW, Olahova M (2020) Mitochondrial OXPHOS biogenesis: co-regulation of protein synthesis, import, and assembly pathways. Int J Mol Sci. https://doi.org/10.3390/ijms21113820
65. Greber S, Lubec G, Cairns N, Fountoulakis M (1999) Decreased levels of synaptosomal associated protein 25 in the brain of patients with Down syndrome and Alzheimer's disease. Electrophoresis 20(4–5):928–934. https://doi.org/10.1002/(SICI)1522-2683(19990101)20:4/5%3c928::AID-ELPS928%3e3.0.CO;2-Z
66. Elias GM, Funke L, Stein V, Grant SG, Bredt DS, Nicoll RA (2006) Synapse-specific and developmentally regulated targeting of AMPA receptors by a family of MAGUK scaffolding proteins. Neuron 52(2):307–320. https://doi.org/10.1016/j.neuron.2006.09.012
67. Kwon SE, Chapman ER (2011) Synaptophysin regulates the kinetics of synaptic vesicle endocytosis in central neurons. Neuron 70(5):847–854. https://doi.org/10.1016/j.neuron.2011.04.001